Phosphorescent Iridium Complexes Activated by Endogenous Zinc as Mitochondrial DNA Nuclease for Stimulation of cGAS-STING Pathway

Zhi-Yuan Li,[†a,c] Long-Bo Yu,[†a,c] Qing-Hua Shen,[a,c] Liang Hao,[a,b,c] Peng Wang,[a,c] Xiao-Xiao Chen,[a,c] Yu-Yi Ling,*[a,c,d] and Cai-Ping Tan *[a,c,d]

[†] These authors contributed equally to this work.

[a] MOE Key Laboratory of Bioinorganic and Synthetic Chemistry, School of Chemistry, Sun Yat-Sen University, Guangzhou 510006, China

[b] The Marine Biomedical Research Institute of Guangdong Zhanjiang, School of-Ocean and Tropical-Medicine, Guangdong Medical University, Zhanjiang, Guangdong, 524023, China.

[c] Guangdong Basic Research Center of Excellence for Functional Molecular Engineering, Guangzhou 510006, China

[d] State Key Laboratory of Anti-Infective Drug Discovery and Development; School of Pharmaceutical Sciences, Sun Yat-sen University, Guangzhou 510006, China

* Corresponding author. E-mail: lingyy@gdmu.edu.cn, tancaip@mail.sysu.edu.cn

Materials and Instruments

Materials

$IrCl_3$ (BIDE, China), 2-phenylpyridine (**ppy**, Energy Chemical, China), 2-(3-methylphenyl)pyridine (**mppy**, BIDE, China), 2-(2',4'-difluorophenyl)pyridine (**dfppy**, BIDE, China), 2-(2-thienyl)pyridine (**thpy**, TCI, China), 4,4'-bis(bromomethyl)-2,2'-bipyridine (BIDE, China), bis(2-pyridylmethyl)amine (Macklin, China), potassium carbonate (Rhawn, China), hydrochloric acid (Guangzhou Chemical Reagent Factory, China), sodium hydroxide (GHTECH, China), 2,2'-bipyridine (**bpy**, InnoChem, China), ammonium hexafluorophosphate (BIDE, China), N,N-Dimethylformamide (DMF, Aladdin Chemical, China), ethylene glycol ethyl ether (Macklin, China), dichloromethane (GHTECH, China), acetonitrile (GHTECH, China), methanol (Macklin, China), dimethyl sulfoxide (DMSO, Sigma Aldrich, USA), deoxyribonucleic acid sodium salt from calf thymus-DNA (CT-DNA, Sigma-Aldrich, USA), phosphate buffered saline (PBS, Sigma Aldrich, USA), Trizol (Takara, Japan). MTT (3-(4,5-dimethylthiazol-2-yl)-2,5-diphenyltetrazolium bromide, Sigma Aldrich, USA), MTDR (MitoTracker Deep Red, Invitrogen, USA), Picogreen (Lumiprobe, USA), ER-Tracker Red (Beyotime, China), LysoTracker™ Red DND-99 (ThermoFisher, China), Z-VAD-FMK (MCE, China), 3-Methyladenine (3-MA, MCE, China), ferrostatin-1 (Fer-1, MCE, China), Liproxstatin-1 (Lip-1, MCE, China) and Necrosulfonamide (NSA, MCE, China) were used as received. All the compounds tested were dissolved in DMSO just before the experiments, and the final concentration of DMSO was kept at 1% (v/v).

The antibodies including GAPDH (AP0063, Bioworld), β-Actin (4970S, CST, USA), γH2A.X (ab81299, abcam), STING (13647S, CST), p-STING (Ser365; 72971S, CST), cGAS (26416-1-AP, Proteintech) and PD-L1 (DF6526, affinity) were purchased from commercial resources. Antibodies against APC anti-mouse CD80 (104714), PE anti-mouse CD86 (105008), FITC anti-mouse CD11c antibody (117305), FITC anti-mouse CD3 (100204), APC anti-mouse CD8a (162306), PE anti-Mouse CD4 antibody were purchased from Biolegend (USA). StarGreen safe Nucleic Acid Dye (10,000×), SYBR Green I Master (Roche, USA) and PrimeScript RT Master Mix (Takara, Japan) were purchased from commercial resources.

Instruments

Electrospray ionization mass spectrometry (ESI-MS) was recorded on a Thermo Scientific LTQ linear ion trap mass spectrometer (USA). The quoted m/z values represented the major peaks in the isotopic distribution. Nuclear magnetic resonance (NMR) spectra were recorded on a Bruker Avance III 400 MHz spectrometer (Germany). Shifts were referenced relative to the internal solvent signals. HPLC was performed on a LCMS-2020 (Shimadzu, Japan). UV/Vis spectra were recorded on a Varian Cary 300 spectrophotometer (USA). Steady-state emission spectra and

lifetime measurements were conducted on a combined fluorescence lifetime and steady state spectrometer (FLS 980, Edinburgh Instruments Ltd, England). Cell imaging experiments were carried out on a confocal microscope (LSM 880, Carl Zeiss, Göttingen, Germany). The concentration of metal ions was measured using Thermo Scientific XSERIES 2 Inductively Coupled Plasma Mass Spectrometry (ICP-MS, USA). Cell viability assay was determined using a microplate spectrophotometer (Infinite M200 Pro, Tecan, Switzerland). Flow cytometric analysis was done using a Beckman Coulter flow cytometer (Beckman Coulter, USA). Polymerase chain reaction (PCR) was performed using a Roche LightCycler 480 Detection System (Roche, USA).

Synthetic Procedures

The chloro-bridged precursors[1] including $[(ppy)_2Ir(\mu\text{-}Cl)]_2$, $[(mppy)_2Ir(\mu\text{-}Cl)]_2$, $[(dfppy)_2Ir(\mu\text{-}Cl)]_2$, $[(thpy)_2Ir(\mu\text{-}Cl)]_2$, the N^N ligand 4,4′-bis(dipicolylaminomethyl)-2,2′-bipyridine (**dDPA-bpy**)[2] were synthesized by literature methods. **Ir1**, **Ir1a**, **Ir3a** and **Ir4a** were synthesized by literature methods with slight modifications, **Ir2**–**Ir4** and **Ir2a** was synthesized by a similarly method. Briefly, the chloro-bridged precursors (0.10 mmol) and **dDPA-bpy** (0.20 mmol) or **bpy** (0.20 mmol) were dissolved in CH_2Cl_2/CH_3OH (2:1, v/v) and heated to reflux for 6 h under an inert atmosphere of nitrogen. The crude product was concentrated under vacuum and purified by silica gel column chromatography (CH_2Cl_2/CH_3OH = 10:1, v/v). After removing the solvent by evaporation, the product was dissolved in a small amount of CH_3OH, then 10-fold excess of NH_4PF_6 saturated aqueous solution was added to obtain the precipitate, which was washed with water and ether.

[Ir(ppy)(dDPA-bpy)](PF$_6$) (Ir1):[3, 4] **Ir1** was obtained as a yellow powder. Yield: 118.5 mg (48.4 %). ^{1}H NMR (400 MHz, DMSO-d_6) δ 8.70 (d, J = 1.8 Hz, 2H), 8.58 (d, J = 5.1 Hz, 4H), 8.27 (d, J = 8.1 Hz, 2H), 7.92 (tt, J = 15.2, 7.0 Hz, 10H), 7.79 – 7.74 (m, 2H), 7.71 (d, J = 5.7 Hz, 2H), 7.67 (d, J = 7.8 Hz, 4H), 7.52 (dd, J = 5.8, 1.4 Hz, 2H), 7.40 (t, J = 6.4 Hz, 2H), 7.17 (ddd, J = 7.4, 5.6, 1.4 Hz, 2H), 7.02 (t, J = 7.3 Hz, 2H), 6.90 (td, J = 7.4, 1.3 Hz, 2H), 6.15 (d, J = 7.5 Hz, 2H), 4.08 (s, 4H), 4.03 (d, J = 3.5 Hz, 8H). ^{13}C NMR (101 MHz, DMSO-d_6) δ 166.83, 155.95, 154.73, 151.69, 150.40, 149.34, 148.65, 145.99, 143.67, 140.42, 138.73, 130.89, 130.17, 127.78, 124.99, 124.66, 124.17, 123.73, 122.20, 119.99, 57.89, 57.19, 40.06, 39.85, 39.64, 39.43, 39.22, 39.02, 38.81. ESI-MS m/z (CH_3OH): calculated for $[M-PF_6]^+$ ($C_{58}H_{50}N_{10}Ir^+$) 1079.38, found 1079.57; $[M-PF_6+H]^{2+}$ ($C_{58}H_{50}N_{10}Ir^{2+}$) 540.20, found 540.86. Purity: 99.06% (by HPLC).
[Ir(mppy)(dDPA-bpy)](PF$_6$) (Ir2):[5] **Ir2** was obtained as a yellow powder. Yield: 171.0 mg (68.3 %). ^{1}H NMR (400 MHz, DMSO-d_6) δ 8.68 (s, 2H), 8.50 (dd, J = 4.9, 1.7 Hz, 4H), 8.21 (d, J = 8.2 Hz, 2H), 7.94 – 7.86 (m, 2H), 7.74 (q, J = 5.6, 3.8 Hz, 10H), 7.60 (d, J = 7.8 Hz, 4H), 7.49 (d, J = 5.7 Hz, 2H), 7.26 (dd, J = 7.5, 5.0 Hz, 4H), 7.13 (t, J = 6.8 Hz, 2H),

6.72 (dd, *J* = 7.9, 1.7 Hz, 2H), 6.01 (d, *J* = 7.6 Hz, 2H), 4.02 (s, 4H), 3.93 (d, *J* = 2.9 Hz, 8H), 2.24 (s, 6H). ^{13}C NMR. ^{13}C NMR (101 MHz, DMSO-d_6) δ 166.90, 157.55, 154.77, 152.47, 149.30, 148.67, 147.94, 146.41, 143.55, 138.47, 137.63, 131.19, 130.69, 130.63, 127.59, 125.47, 123.86, 123.60, 122.69, 119.76, 59.35, 56.92, 40.06, 39.86, 39.65, 39.44, 39.23, 39.02, 38.81, 20.56. ESI-MS *m/z* (CH_3OH): calculated for $[M-PF_6]^+$ ($C_{60}H_{54}N_{10}Ir^+$) 1107.42, found 1107.56; $[M-PF_6+H]^{2+}$ ($C_{60}H_{55}N_{10}Ir^{2+}$) 554.21, found 554.73. Purity: 97.42% (by HPLC).

[Ir(dfppy)(dDPA-bpy)](PF$_6$) (Ir3) :[5] **Ir3** was obtained as a pale yellow powder. Yield: 151.4 mg (58.4 %). ^{1}H NMR (400 MHz, DMSO-d_6) δ 8.70 (s, 2H), 8.62 (d, *J* = 5.0 Hz, 4H), 8.30 (d, *J* = 8.6 Hz, 2H), 8.05 (t, *J* = 7.9 Hz, 2H), 7.94 (q, *J* = 7.8, 6.5 Hz, 4H), 7.82 – 7.76 (m, 4H), 7.68 (d, *J* = 8.0 Hz, 4H), 7.59 (d, *J* = 5.9 Hz, 2H), 7.51 – 7.41 (m, 4H), 7.25 (t, *J* = 6.7 Hz, 2H), 6.98 (ddd, *J* = 12.1, 9.4, 2.4 Hz, 2H), 5.58 (dd, *J* = 8.3, 2.4 Hz, 2H), 4.12 (s, 4H), 4.06 (d, *J* = 4.3 Hz, 8H). ^{13}C NMR (101 MHz, DMSO-d_6) δ 162.77, 162.70, 162.00, 161.56, 161.43, 159.41, 159.28, 155.86, 154.50, 152.37, 149.75, 149.35, 145.87, 140.68, 140.05, 128.13, 127.45, 124.75, 124.40, 123.83, 123.47, 123.28, 113.19, 113.01, 99.27, 98.99, 57.73, 57.14, 40.06, 39.85, 39.64, 39.44, 39.23, 39.02, 38.81. ESI-MS *m/z* (CH_3OH): calculated for $[M-PF_6]^+$ ($C_{58}H_{46}N_{10}F_4Ir^+$) 1151.34, found 1151.55; $[M-PF_6+H]^{2+}$ ($C_{58}H_{47}N_{10}F_4Ir^{2+}$) 576.18, found 576.62. Purity: 97.68% (by HPLC).

[Ir(thpy)(dDPA-bpy)](PF$_6$) (Ir4):[5] **Ir4** was obtained as an orange powder. Yield: 68.6 mg (27.8 %). ^{1}H NMR (400 MHz, DMSO-d_6) δ 8.68 (s, 2H), 8.56 (d, *J* = 5.0 Hz, 4H), 7.89 – 7.72 (m, 10H), 7.66 (dd, *J* = 8.7, 4.8 Hz, 8H), 7.42 (d, *J* = 5.9 Hz, 2H), 7.36 (t, *J* = 6.3 Hz, 4H), 6.97 (t, *J* = 6.6 Hz, 2H), 6.14 (d, *J* = 4.7 Hz, 2H), 4.09 (s, 4H), 4.02 (s, 8H). ^{13}C NMR (101 MHz, DMSO-d_6) δ 162.94, 156.64, 154.87, 152.44, 152.19, 149.88, 149.18, 146.86, 139.25, 136.01, 130.88, 130.11, 127.86, 124.22, 124.02, 123.27, 120.84, 118.24, 58.58, 57.08, 40.06, 39.85, 39.64, 39.43, 39.22, 39.02, 38.81. ESI-MS *m/z* (CH_3OH): calculated for $[M-PF_6]^+$ ($C_{54}H_{46}N_{10}S_2Ir^+$) 1091.30, found 1091.70; $[M-PF_6+H]^{2+}$ ($C_{54}H_{47}N_{10}S_2Ir^{2+}$) 546.15, found 546.85. Purity: 97.57% (by HPLC).

[Ir(ppy)(bpy)](PF$_6$) (Ir1a):[6] **Ir1a** was obtained as a yellow powder. Yield: 113.3 mg (70.6 %). ^{1}H NMR (400 MHz, DMSO-d_6) δ 8.88 (d, *J* = 8.2 Hz, 2H), 8.27 (ddd, *J* = 8.0, 4.7, 1.7 Hz, 4H), 7.97 – 7.90 (m, 4H), 7.87 (dd, *J* = 5.4, 1.6 Hz, 2H), 7.70 (ddd, *J* = 7.7, 5.4, 1.1 Hz, 2H), 7.64 – 7.60 (m, 2H), 7.16 (ddd, *J* = 7.3, 5.7, 1.4 Hz, 2H), 7.02 (td, *J* = 7.5, 1.2 Hz, 2H), 6.91 (td, *J* = 7.4, 1.3 Hz, 2H), 6.19 (dd, *J* = 7.7, 1.2 Hz, 2H). ^{13}C NMR (101 MHz, DMSO-d_6) δ 166.70, 155.26, 150.35, 149.73, 148.78, 143.69, 139.57, 138.68, 130.95, 130.15, 128.59, 124.99, 124.91, 123.84, 122.18, 119.95, 40.03, 39.82, 39.61, 39.40, 39.19, 38.99, 38.78. ESI-MS *m/z* (CH_3OH): calculated for $[M-PF_6]^+$ ($C_{32}H_{24}N_4Ir^+$) 657.16, found 657.31. Purity: 98.09% (by HPLC).

[Ir(mppy)(bpy)](PF$_6$) (Ir2a):[5] **Ir2a** was synthesized by a similarly method and obtained as yellow powder. Yield: 86.4 mg (52.0 %). ^{1}H NMR (400 MHz, DMSO-d_6) δ 8.87 (dd, *J* = 8.0, 1.2 Hz, 2H), 8.30 – 8.16 (m, 4H), 7.95 – 7.86 (m, 4H),

7.74 (d, *J* = 1.8 Hz, 2H), 7.70 (ddd, *J* = 7.6, 5.4, 1.2 Hz, 2H), 7.58 (ddd, *J* = 5.8, 1.6, 0.8 Hz, 2H), 7.13 (ddd, *J* = 7.3, 5.9, 1.4 Hz, 2H), 6.78 – 6.67 (m, 2H), 6.05 (d, *J* = 7.7 Hz, 2H), 2.24 (s, 6H). ^{13}C NMR (101 MHz, DMSO-d_6) δ 166.79, 155.28, 149.81, 148.73, 146.26, 143.55, 139.45, 138.51, 131.21, 130.76, 130.70, 128.55, 125.50, 124.85, 123.64, 119.79, 40.03, 39.82, 39.61, 39.40, 39.19, 38.99, 38.78, 20.55. ESI-MS *m/z* (CH_3OH): calculated for $[M-PF_6]^+$ ($C_{34}H_{28}N_4Ir^+$) 685.19, found 685.33. Purity: 99.92% (by HPLC).

[Ir(dfppy)(bpy)](PF$_6$) (Ir3a):[7] Complex **Ir3a** was synthesized by the literature methods and obtained as pale yellow powder. Yield: 132.4 mg (75.7 %). ^{1}H NMR (400 MHz, DMSO- d_6) δ 8.90 (d, *J* = 8.2 Hz, 2H), 8.32 (ddd, *J* = 10.6, 8.2, 2.1 Hz, 4H), 8.04 (td, *J* = 7.9, 1.7 Hz, 2H), 7.97 – 7.89 (m, 2H), 7.71 (ddd, *J* = 11.1, 5.5, 1.3 Hz, 4H), 7.25 (ddd, *J* = 7.4, 5.8, 1.4 Hz, 2H), 6.99 (ddd, *J* = 12.1, 9.4, 2.3 Hz, 2H), 5.62 (dd, *J* = 8.4, 2.4 Hz, 2H). ^{13}C NMR (101 MHz, DMSO-d_6) δ 163.60, 163.52, 162.65, 162.61, 161.91, 161.83, 161.52, 161.43, 159.79, 159.71, 155.03, 154.43, 154.39, 150.19, 149.52, 140.13, 139.96, 129.01, 127.49, 127.46, 125.14, 125.08, 124.45, 123.36, 123.24, 113.20, 113.08, 99.15, 98.97, 98.79, 64.80, 39.86, 39.72, 39.58, 39.44, 39.30, 39.16, 39.02, 15.06. ESI-MS *m/z* (CH_3OH): calculated for $[M-PF_6]^+$ ($C_{32}H_{20}N_4F_4Ir^+$) 729.12, found 729.32. Purity: 98.27% (by HPLC).

[Ir(thpy)(bpy)](PF$_6$) (Ir4a):[8] Complex **Ir4a** was synthesized by the literature methods and obtained as orange powder. Yield: 102.6 mg (63.0 %). ^{1}H NMR (400 MHz, DMSO-d_6) δ 8.87 (d, *J* = 8.2 Hz, 2H), 8.28 (td, *J* = 7.9, 1.6 Hz, 2H), 7.88 – 7.79 (m, 4H), 7.75 (dd, *J* = 11.7, 6.6 Hz, 4H), 7.66 (d, *J* = 4.8 Hz, 2H), 7.52 (d, *J* = 5.8 Hz, 2H), 6.96 (ddd, *J* = 7.4, 5.8, 1.7 Hz, 2H), 6.18 (d, *J* = 4.7 Hz, 2H). ^{13}C NMR (101 MHz, DMSO-d_6) δ 162.82, 155.42, 152.27, 150.36, 149.29, 139.66, 139.25, 136.04, 130.83, 130.18, 128.73, 124.85, 120.93, 118.21, 40.03, 39.82, 39.61, 39.41, 39.20, 38.99, 38.78. ESI-MS *m/z* (CH_3OH): calculated for $[M-PF_6]^+$ ($C_{28}H_{20}N_4S_2Ir^+$) 669.08, found 669.33. Purity: 99.36% (by HPLC).

HPLC analysis

Ir(III) complexes (100 μM) were dissolved in methanol. The injection volume is 10 μL each time and the detection wavelength is 280 nm. Water (with 0.1% trifluoroacetic acid) and methanol were used as the mobile phase A and B, respectively. Flow rate: 1 mL min^{-1}. 2−13 min: 20% B−90% B; 13−15 min: 90% B; 15−20 min: 90% B−20% B. The purity of the Ir(III) complexes was calculated by calculating the integraated peak area at 280 nm.

Photophysical properties of complexes

UV/vis absorption spectra, emission spectra and emission decay curves of the Ir(III) complexes (20 μM) were measured in degassed PBS (pH 7.4), CH_3CN and CH_2Cl_2 at 298 K. The fluorescent quantum yields were calculated

using $[Ru(bpy)_3](PF_6)_2$ as the standard.[9-11] Decay traces were best fitted to a bi-exponential decay model using the equation:

$$R(t) = A + B_1 exp(-t/\tau_1) + B_2 exp(-t/\tau_2)$$

And the phosphorescence lifetimes were calculated by the equation:

$$\tau_{av} = \frac{B_1\tau_1^2 + B_2\tau_2^2}{B_1\tau_1 + B_2\tau_2}$$

λ_{ex} = 405 nm. λ_{em} = 610 nm.

Lipophilicity

The Log $P_{o/w}$ values of the Ir(III) complexes were determined according to a reported procedure[12]. Log $P_{o/w}$ is defined as the logarithmic ratio of Ir(III) complexes in n-octanol to that in the aqueous phase.

Binding properties of complexes with Zn^{2+}

Phosphorescence selectivity experiment

The emission spectra and emission decay curves of **Ir1**–**Ir4** (20 μM) were measured with various essential metal ions (40 mM K^+, Na^+, or 40 μM Ca^{2+}, Mg^{2+}, Mn^{2+}, Fe^{3+}, Fe^{2+}, Ni^{2+}, Co^{2+}, Cr^{3+}, Cu^+ and Cu^{2+}) and common biomolecules (200 μM GSH, 1 mg BSA, 40 μM ctDNA, 200 μg yeast RNA). All the metal ions were attained from degassed aqueous solutions of metal chlorides, expect for Cu^+ was prepared from the mixed solution of $CuSO_4$ and L-ascorbic acid sodium salt. Then, 40 μM $ZnCl_2$ was added into the mixture solutions and the emission spectra and emission decay curves were measured again.

UV/Vis and phosphorescence titration

The UV/vis and the emission spectra of **Ir1**–**Ir4** (20 μM) were measured with increasing amounts of $ZnCl_2$ (0–2.0 equiv.) in degassed PBS. The phosphorescence lifetime profiles of **Ir1**–**Ir4** titrated with Zn^{2+} were also measured in the same way and analyzed with a bi-exponential decay model. λ_{ex} = 405 nm.

The solution was evenly mixed and balanced for 3 min after each titration. The Benesi-Hildebrand equation was used for the fitting calculation:[13]

$$\frac{1}{A - A_0} = \frac{1}{K(A_0 - A_e)[M]^n} + \frac{1}{A_0 - A_e}$$

$$\frac{1}{F - F_0} = \frac{1}{K(F_0 - F_e)[M]^n} + \frac{1}{F_0 - A_e}$$

where A_0, A and A_e are the absorption values of **Ir1**–**Ir4** in the absence, presence and saturated with Zn^{2+}, while F represents the emission intensities. n is the binding ratio of **Ir1**–**Ir4** with Zn^{2+}, which equals 2.0 proved by Job's Plots. The inset plots of $1/[A - A_0]$ against $1/[Zn^{2+}]^2$ and $1/[F - F_0]$ against $1/[Zn^{2+}]^2$ were built, and the binding constant K was obtained by dividing the intercept by the slope and shown in Figure 1 and S31.

The emission spectra and emission decay curves of control complexes were also measured in the absence and presence of $ZnCl_2$. λ_{ex} = 405 nm.

Job's plot analysis

The Ir(III) complexes and Zn^{2+} in different proportions were mixes in PBS, and the total concentration of Ir(III) complexes and Zn^{2+} was kept at 30 μM. The emission spectra of the resulting solution was then measured. The binding stoichiometry was determined from the x-axis values of the two linearly fitted intercepts of F against ([Ir]/([Ir] + $[Zn^{2+}]$) curve, where F is emission intensity of the solution at a constant wavelength. λ_{ex} = 405 nm.

Density-functional theory (DFT) and time-dependent density-functional theory (TDDFT) calculation

The ground state and excited state optimizations of **Ir1** and **Ir1-Zn_2** were calculated using the DFT and TDDFT methods on Gaussian09 program. DFT and TDDFT calculations were performed at the PBE0//6-31G*&LanL2DZ level. The 6-31G* basis set was used for the C, H, O, N atoms, and the LANL2DZ was used for the Ir atom.

DNA binding experiments

Ir1-Zn_2 was prepared by mixing 1.0 equiv. of **Ir1** dissolved in DMSO and 2.0 equiv. of $ZnCl_2$ aqueous solution.

UV-Vis titration

The UV-Vis absorption spectra of **Ir1**/**Ir1-Zn_2** (20 μM) were measured in Tri-HCl buffer (10 mM Tris-HCl, 100 mM NaCl, pH 7.4) by varying the concentration of calf thymus-DNA (ct-DNA; 0–80 μM). After each titration, the solution is evenly mixed and balanced for 3 min before measurement. The absorbance at 405 nm was used to calculate the binding constants. The binding constants (K_b) of **Ir1**/**Ir1-Zn_2** towards ct-DNA were calculated according to the function below.[14]

$$\frac{\varepsilon_a - \varepsilon_f}{\varepsilon_b - \varepsilon_f} = (b - (b^2 - 2K_b{}^2 C_t[DNA]/s)^{1/2})/2K_b C_t$$

$$b = 1 + K_b C_t + K_b[DNA]/2s$$

where ε_a, ε_f and ε_b are the apparent, free, and bound ligand extinctions, respectively. [DNA] represents the DNA concentration in nucleobase. C_t represents concentration of the Ir(III) complexes.

Fluorescence titration

The emission spectra of **Ir1**/**Ir1-Zn$_2$** (20 μM) were measured in Tri-HCl buffer (10 mM Tris-HCl, 100 mM NaCl, pH 7.4) by varying the concentration of ct-DNA (0–80 μM). After each titration, the solution is evenly mixed and balanced for 3 min before measurement. The fluorescence intensity at maximum emission wavelength was used to calculate the binding constant (K_b) using the Stern-Volmer function:[15]

$$lg\frac{F - F_0}{F} = lgK_b + nlg[DNA]$$

where F_0 and F are the emission intensities of **Ir1**/**Ir1-Zn$_2$** in presence and presence of [DNA] and n is the number of binding sites. λ_{ex} = 405 nm.

Agarose gel electrophoresis

To avoid the chelation of Zn^{2+} by EDTA towards $ZnCl_2$, the pBR322 plasmid (250 ng) was extracted and purified by DiaSpin Plasmid Mini-Preps Kit (Sangon Biotech, B110091-0050, China), and was stocked in DEPC water at -20 °C. The plasmid was incubated with at the indicated concentrations of **Ir1** and $ZnCl_2$ for 8 h at 37 °C in Tris-HCl buffer (pH 7.4, 100 mM NaCl). Gel electrophoresis of DNA was performed on a 1% agarose gel. The gel was stained with StarGreen safe Nucleic Acid Dye and imaged on FluorChem M (ProteinSimple, Santa Clara, CA). The raw images of gels are shown in Figure S52.

Viscosity measurements

An Ubbelohde viscometer was used for the measurements of viscosities, and the temperature was maintained at room temperature. The DNA concentration was kept constant (15 μM) in all samples, while the complex concentration was increased from 0-30 μM. Flow time was measured with a digital stopwatch and the mean value was calculated from at least 3 times measurements. Viscosity value (η) was calculated from the expression $(t - t_0)/t_0$, where t is the flow time of DNA-containing solution and t_0 is the flow time of buffer alone. Viscosity data were presented as $(\eta/\eta_0)^{1/3}$ versus concentration ratio of [complex]/[DNA], where η is the viscosity of DNA in the presence of **Ir1-Zn$_2$**/**Ir1**, and η_0 is the viscosity of DNA alone.

Molecular docking

The crystal data of a DNA-ligand complex (PDB: 5t4w) was used for docking studies. The original ligand and water were removed by PyMOL[16] and the DNA was prepared by Accelrys Discovery Studio 2.5.5. The stuctures of **Ir1**/**Ir1-Zn_2** were optimized using DFT calculations by Gaussian09 package at B3LYP/6-31g (d, p) level. Using the optimized **Ir1**/**Ir1-Zn_2** structure, the partial atomic charges were obtained by restrained electrostatic potential (RESP)[17] calculating with Gaussian 09 package at the level of HF/6-31g*. The docking calculations were then performed by the AutoDock 4 suite of programs,[18] using ligand flexible docking approach that allows ligand flexibility. The Lamarckian genetic algorithm[19] was chosen as the search protocol using the default parameters except for number of GA runs (ga_run = 100) and the maximum number of energy evaluations (ga_num_evals = 25,000,000). The docking model with the lowest docked free energy was selected for further investigated in this article. And then, the docking complex was optimized with minimization protocols by Accelrys Discovery Studio 2.5.5 The displaying images were rendered with PyMOL or Accelrys Discovery Studio 2.5.5. The hydrophobic contacts were presented by LigPlot$^+$ v.1.4.5 software[20] with hydrophobic-any contact distance 2.9-4.5.

Cell lines and culture conditions

MDA-MB-231 cells, MCF-7 cells, MCF-10A cells, 4T1 cells and HeLa cells were obtained from Experimental Animal Center of Sun Yat-Sen University (Guangzhou, China). Cells were cultured in DMEM (Dulbecco's modified Eagle's medium, Gibco BRL) containing 10% FBS (fetal bovine serum, Gibco BRL), 100 μg mL^{-1} streptomycin, and 100 U mL^{-1} penicillin (Gibco BRL). The cells were cultured in tissue culture flasks in a humidified incubator at 37 °C, under an atmosphere of 5% CO_2 and 95% air. In each experiment, cells treated with vehicle DMSO (1%, v/v) were used as the reference group.

Antiproliferative assay

The antiproliferative activities of the tested compounds against MDA-MB-231, MCF-7, MCF-10A, 4T1 cells and Hela cells were determined by MTT assay as previously described.[21] Briefly, the cell suspension was inoculated into the 96 well plates with about 10^4 cells per well. After the cultured cells in the 96-well plates were grown to confluence. The cells were incubated with gradient concentrations of the tested compounds for 68 h at 37 °C. The media were refreshed and 20 μL of MTT solution was then added to each well, and the plates were incubated for an additional 4 h. The medium was carefully removed, and DMSO was added (150 μL per well). The plates were incubated for 3 min with shaking. The absorbance at 595 nm was measured using a microplate reader (Infinite M200 Pro, Tecan,

Switzerland). IC_{50} values (compound concentration that produces 50% of cell growth inhibition) were calculated from curves constructed by plotting cell survival (%) versus drug concentration (μM). Each experiment was repeated at least three times to gain the mean values.

ICP-MS measurement

The cellular iridium content was measured by ICP-MS using the protocol we previously reported.[22] Briefly, MDA-MB-231 cells were incubated with **Ir1/Ir2/Ir3/Ir4/Ir1a/Ir2a/Ir3a/Ir4a** (2 μM) for 1 h, the cells were collected and counted. To detect zinc contents of MDA-MB-231 cells and Hela cells, cells were directly collected and counted. Mitochondria were isolated according to the protocol provided by the Cell Mitochondria Isolation Kit (Solarbio, SM0020). ER were isolated according to the protocol provided by the Cell ER Isolation Kit (BB-36051-50T, beibo). Cell nucleus were isolated according to the protocol provided by the Nuclear and Cytoplasmic Protein Extraction Kit (P0028, Beyotime). The collected cells, mitochondria and cytoplasm, ER and nucleus were added HNO_3 (65%, 500 μL) and incubate at room temperature for 24 h. The solution was then diluted to a final volume of 5 mL with deionized water. The concentration of iridium/zinc was determined by XSERIES 2 inductively coupled plasma mass spectrometer (ICP-MS). The standard curve (R^2 > 0.999) was determined using a gradient concentration of iridium/zinc standard solution (1000 mg mL^{-1}).

Colocalization studies

MDA-MB-231 cells were seeded into confocal dishes and incubated at 37 °C for 24 h. The cells were treated with **Ir1–Ir4** or **Ir1a–Ir4a** (2 μM) for the corresponding period of time and then stained with MTDR (100 nM) for 15 min. Then cells were imaged by confocal microscopy immediately. **Ir1–Ir4** and **Ir1a–Ir4a**: λ_{ex} = 405 nm; λ_{em} = 600 ± 20 nm. λ_{ex} = 633 nm. MTDR: λ_{em} = 660 ± 10 nm.

For the colocalization studies of **Ir1** with ETR and LTR in MDA-MB-231 cells, cells were treated with **Ir1** (2 μM, 60 min) and then incubated with ETR (1 μM, 15 min) or LTR (1 μM, 15 min). **Ir1**: λ_{ex} = 405 nm; λ_{em}= 600 ± 20 nm. ETR: λ_{ex} = 561 nm. λ_{em} = 615 ± 20 nm. LTR: λ_{ex} = 561 nm. λ_{em} = 615 ± 20 nm.

PicoGreen staining with confocal microscopy

MDA-MB-231 cells were seeded into confocal dishes and incubated at 37 °C for 24 h. After treated with **Ir1/Ir1a** (2 μM) for 15 min/30 min, the cells were stained with PicoGreen and MTDR for 15 min and imaged by confocal microscopy. **Ir1/Ir1a**: λ_{ex}= 405 nm; λ_{em}= 600 ± 20 nm. PicoGreen: λ_{ex} = 488 nm, λ_{em} = 520 ± 20 nm. MTDR: λ_{ex} = 633

nm. λ_{em} = 660 ± 10 nm.

Two-photon phosphorescence lifetime microscopy (TPPLM)

MDA-MB-231 cells were seeded into confocal dishes and incubated at 37 °C for 24 h. After treated with **Ir1** (2 μM) for 15 min/60 min/6 h, the cells were imaged by confical microscopy. The experiments were performed on a Zeiss LSM880 equipped with a Chameleon Vision-S ultrafast laser, Coherent, inc.. The data were analyzed by the Becker & Hickl SPCImage data analysis software. λ_{ex} = 810 nm (two-photon); λ_{em} = 600 ± 20 nm.

RNA-Seq analysis

The experiment was performed as previously described.[21] MDA-MB-231 cells were seeded in 10 cm plates for 24 h and treated with **Ir1** (2 μM, 6 h). Then, cells were harvested and total RNA was extracted by Trizol reagent (Takara, Japan). RNA-seq was performed by Biomarker Technologies. The quality of RNA was measured by the kaiaoK5500® Spectrophotometer (Kaiao, Beijing, China). The integrity of RNA was measured using RNA Nano 6000 Assay Kit (Agilent Technologies, CA, USA). Samples with RNA integrity number no less than 7 were used for sequencing. RNA-seq libraries were constructed using Illumina TruSeq RNA Sample kit (Illumina, San Diego, CA). Insert size was measured by the Agilent Bioanalyzer 2100 system (Agilent Technologies, CA, USA), and qualified insert size was accurate quantification using StepOnePlus™ Real-Time PCR System. All the libraries were sequenced by Illumina platform with paired-end 150 bp reads length. All the sequencing reads were mapped to human reference genome sequence (GRCh37/hg19 assembly) by TopHat (Version 2.0.6). Genes with false discovery rate of < 0.05 and > 200 bp were considered as differentially expressed. Gene Set Enrichment Analysis (GSEA) was performed following the standard procedure (http://www.broadinstitute.org/gsea/doc/GSEAUserGuideFrame.html) as described by GSEA user guide).

RT-qPCR

The experiment was performed as previously described.[21, 23] MDA-MB-231 cells were seeded into 6-well plates and incubated at 37 °C for 24 h. The cells were treated with **Ir1** (2 μM, 6 h). The cells were washed with PBS, RNA was isolated using the Trizol reagent (1 mL). Reverse transcription to cDNA was carried out using the PrimeScript RT Master Mix (Takara, Japan). RT-PCR was performed on a Roche LightCycler 480 Detection System (Roche, USA) using SYBR Green I Master (Roche, USA) kit according to manufacturer's instructions. The following cycling conditions were applied for the RT-qPCR experiment: denature 95 °C for 10 min, followed by 40 cycles of 95 °C for

10 s, 60 °C for 15 s and 72 °C for 20 s. GAPDH was used as the reference gene. The primer sequences are listed in Table S13.

Transmission electron microscopy (TEM)

The experiment was performed as previously described.[21] MDA-MB-231 cells were treated with **Ir1** (2 μM, 6 h). The cells were collected and fixed with 2.5% glutaraldehyde, treated with osmium tetroxide, stained with uranyl acetate and lead citrate, and visualized under a transmission electron microscope (JEM 100 CX, JEOL, Tokyo, Japan). Images were photographed using the Eversmart Jazz program (Scitex). Cell treated with vehicle (1% DMSO) were kept as controls.

Antiproliferation and cytotoxicity assay

MDA-MB-231 cells cultured in 96 well plates were pretreated with the inhibitors (Nec-1: 100 μM; 3-MA: 0.5 mM; z-VAD-FMK: 5 μM; NSA: 5 μM; Lip-1: 200 nM; Fer-1: 10 μM) for 1 h, then incubated with **Ir1** (10 μM) for 24 h. Cell viabilities were detected as described above.

Cellular ROS detection

MDA-MB-231 cells were seeded into 6-well plates and incubated at 37 °C for 24 h. Then cells were treated with **Ir1** at the indicated concentrations for 6 h. Then, the cells were harvested and incubated with DCFH-DA (10 μM) for 15 min at 37 °C in the dark. The samples were then analyzed by flow cytometry or confocal microscopy. DCF: λ_{ex} = 488 nm; λ_{em} = 530 ± 20 nm.

Mitochondrial membrane potential assays

MDA-MB-231 cells were seeded into 6-well plates and incubated at 37 °C for 24 h. Then cells were treated with **Ir1** (1 μM/2 μM/4 μM) at the indicated concentrations for 6 h. Then, the cells were collected and suspended in JC-1 staining buffer solution at 37 °C for 20 min. FlowJo software was used to analyze the data. JC-1: λ_{ex} = 488 nm, λ_{em} = 530 ± 30 nm (Green) and 590 ± 30 nm (Red).

MtDNA damage

Determination of mtDNA copy number and amplification

The experiment was performed as previously described.[24] MDA-MB-231 cells were treated with **Ir1** (2 μM) for 24

h. DNA was extracted and purified by AxyPrep Blood gDNA MiniPrep kit. For mtDNA amplification measurement, DNA was isolated and a SequalPrep™ Long PCR Kit was used to amplify the 8.9 kb segment of mtDNA and the 12.2 kb segment of nucDNA. qPCR was performed using SYBR Green I Master on a Roche LightCycler 480 Detection System. The primer sequences are listed at Table S13.

Gel electrophoresis

The experiment was performed as previously described.[24] MDA-MB-231 cells were treated with **Ir1** (2 μM) for 24 h. MtDNA was extracted and purified by the Quick-gDNATM MiniPrep kit from isolated mitochondria. Gel electrophoresis of mtDNA was performed on a 1% agarose gel. After stained with Gel-Red, the image was captured by a FluorChem M imaging station. The raw images of gels are shown in Figure S52.

RT-qPCR of mtDNA-encoded genes

The experiment was performed as previously reported[24] and described above. MDA-MB-231 cells were treated with **Ir1** (2 μM, 24 h). β-actin was used as the housekeeping genes to normalize the data. The primer sequences are listed at Table S13.

Western blotting

MDA-MB-231 cells were treated with **Ir1** (0, 2 and 4 μM) for 24 h. For ROS scavenge, the cells were treated with N-acetylcysteine (NAC,10 mM) and **Ir1** (2 μM) for 24 h. Intracellular proteins were extracted by differential centrifugation (cell lysis buffer, PMSF, 1 mM). Extracted proteins were quantified using the BCA protein detection kit, electrophoresed in 10% polyacrylamide gels and transferred to PVDF membranes, which were blocked with QuickBlock™ and incubated overnight at 4 °C with primary antibodies to SLC39A5, MT1X, p-STING, STING, cGAS, γH2A.X, PD-L1, GADPH and β-actin, followed by incubation with the appropriate horseradish peroxidaseconjugated secondary antibody. After washing 3 times with PBST, the PVDF membrane was incubated with the secondary antibody Goat Anti-Rabbit IgG H&L (HRP) for 2 hours and shoot with chemiluminescence kit. The gray scale of protein blot was measured by Image J. The raw images of blots are shown in Figure S53.

***In vivo* antitumor evaluation**

The animal experiment procedures were approved by the Institutional Animal Care and Use Committee of Sun Yat-sen University and performed in accordance with the ethical guidelines of Sun Yat-sen University. The accreditation

number is SYSU-IACUC-2025-000460. The BALB/C female mice were randomly divided into 7 groups (Control, cisplatin, BMS-1, **Ir1**, **Ir1a**, **Ir1** + BMS-1, and **Ir1a** + BMS-1). 4T1 cells (1×10^6 cells/100 μL PBS) were subcutaneously inoculated on the right side of BALB/C mice as the primary tumor. When the primary tumors reach the size of 100 mm^3, **Ir1** (5 mg kg^{-1}), BMS-1 (5 mg kg^{-1}), or cisplatin (5 mg kg^{-1}) were intratumorally injected into the primary tumor on day 0, and 4T1 cells (1×10^6 cells/100 μL PBS) were inoculated on the contralateral side of the mice one week later, as a recurrent tumor. The mice were monitored for tumor volumes and body weight every 2 days. The tumor volume (V) was calculated as $V = W^2 \times L/2$, where W is the width and L is the length of the tumor. After 18 days, the mice were sacrificed, and the viscera and tumor were dissected out.

Flow cytometry

For flow cytometric analysis, The recurrent tumors of three mice were took in each group, and cut into small pieces and digested with collagenase IV (1 mg mL^{-1}) and DNaseI (0.1 mg mL^{-1}) at 37 °C for 1 h, then large pieces of tissue were filtered through nylon cell filters to obtain a single-cell suspension. After removing red blood cells with red blood cell lysis buffer, the resulting cells were stained with anti-CD3-mouse-FITC, anti-CD8a-mouse-APC, anti-CD4-mouse-PE, anti-CD11c-mouse-FITC, anti-CD80-mouse-APC, anti-CD86-mouse-PE, and finally detected and analyzed using BD FACS Calibur™ flow cytometer.

Hematoxylin-eosin (H&E) staining

The tumors and major organs (including heart, kidney, liver, lung, and spleen) were resected and fixed with 4% paraformaldehyde. The samples of major organs were then embedded in paraffin, sliced and H&E staining, and then observed and photographed under a Zeiss AxioImager. Z2 microscope (Germany).

Immunofluorescence (IF)/ Immunohistochemistry (IHC)

The mouse tumors were initially dissected, and the central portion was excised and fixed in 4% paraformaldehyde. Following fixation, the tissue samples were embedded in paraffin and sectioned using a microtome to produce unstained sections, which can be stored long-term for subsequent immunofluorescence/immunohistochemistry.

Biodistribution of Ir1 in mice

4T1 cells (1×10^6 cells/100 μL PBS) were subcutaneously inoculated on the one side of BALB/C mice, and fed until the size of tumors reached 100 mm^3. mice were randomized into 3 groups (24 h, 48 h, 7 days). Then **Ir1** (5 mg kg^{-1})

were injected via intertumoral injection into tumor-bearing mice. Then the fresh mouse blood, heart, liver, spleen, lung, kidney and tumor of the mice (n = 3) was collected at 24 h, 48 h, 7 days post-administration. The tissues and tumors were minced, then were dissolved in HNO_3 (65%, 2 mL) and incubate at room temperature for 24 h. The blood samples were also dissolved in HNO_3 (65%, 1 mL) and incubate at room temperature for 24 h. The solution was then diluted to a final volume of 50 mL with deionized water. The concentration of iridium was determined by XSERIES 2 inductively coupled plasma mass spectrometer (ICP-MS). The standard curve ($R^2 > 0.999$) was determined using a gradient concentration of iridium standard solution (1000 mg mL^{-1}).

Long-term toxicity assessment of Ir1 in mice

4T1 cells (1×10^6 cells/100 μL PBS) were subcutaneously inoculated on the one side of BALB/C mice, and fed until the size of tumors reached 100 mm^3. mice were randomized into 3 groups (24 h, 48 h, 7 days). Then **Ir1** (5 mg kg^{-1}) were injected via intertumoral injection into tumor-bearing mice. Then the fresh mouse blood (n = 3) was collected at 24 h, 48 h, 7 days post-administration. Blood was subsequently collected for routine blood tests.

Statistical analysis

All biological experiments were performed at least twice with triplicates in each experiment. Representative results were depicted in this report and data were presented as means ± standard deviations (SD).

Supporting Schemes, Figures and Tables

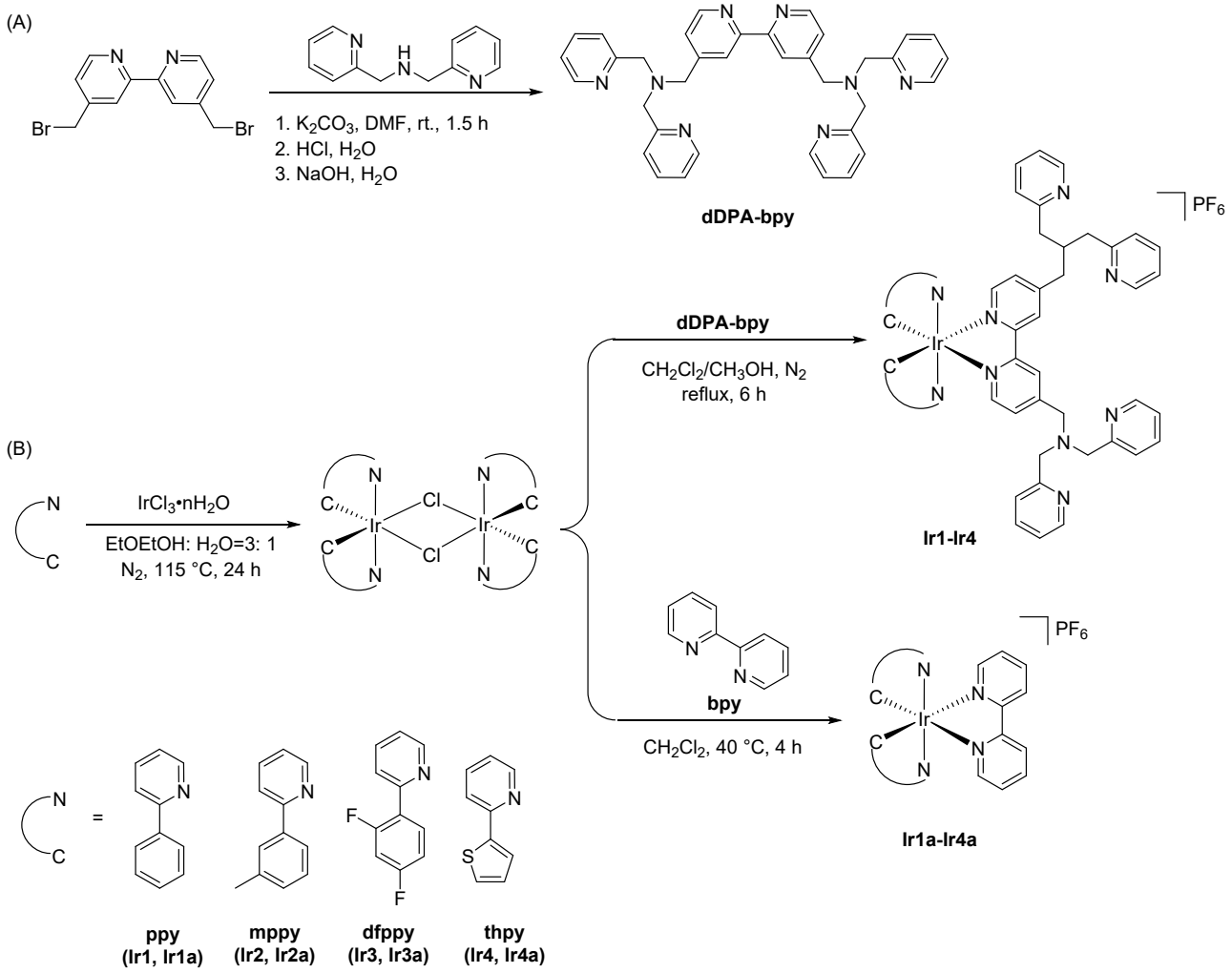

Scheme S1. Synthetic routes of **dDPA-bpy** (A) and Ir(III) complexes (B).

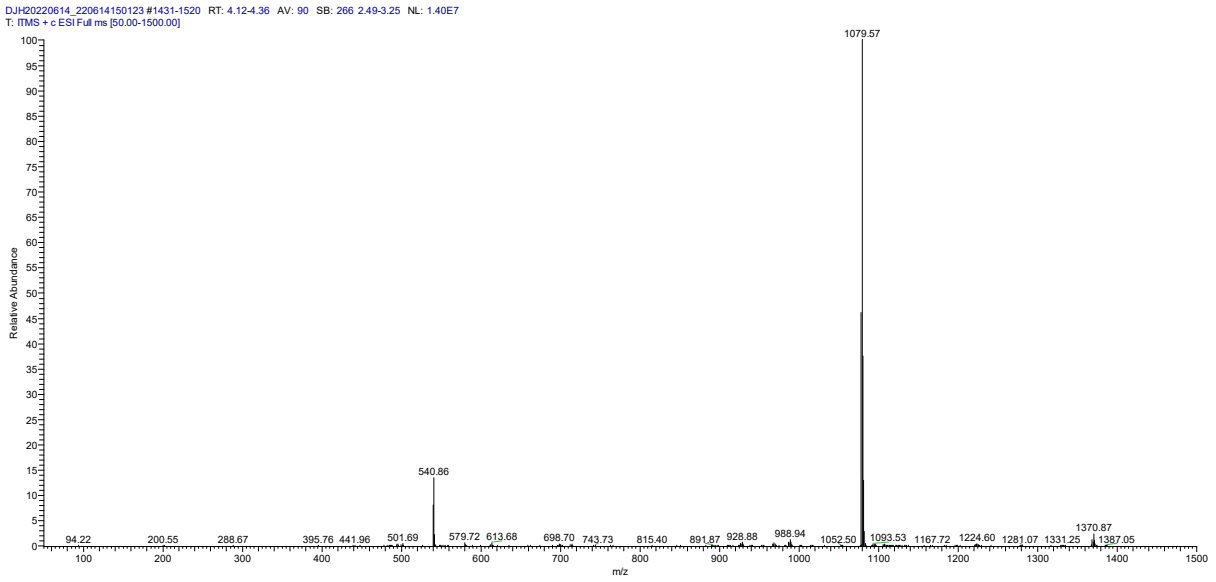

Figure S1. ESI-MS spectrum of **Ir1**.

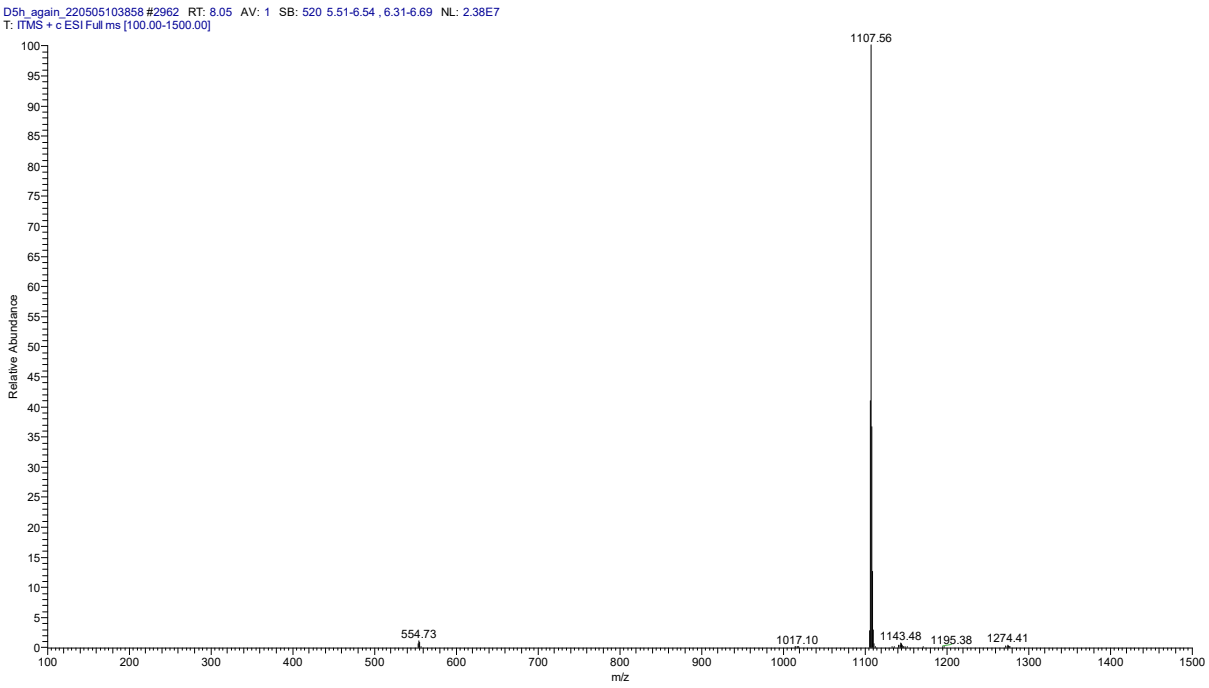

Figure S2. ESI-MS spectrum of **Ir2**.

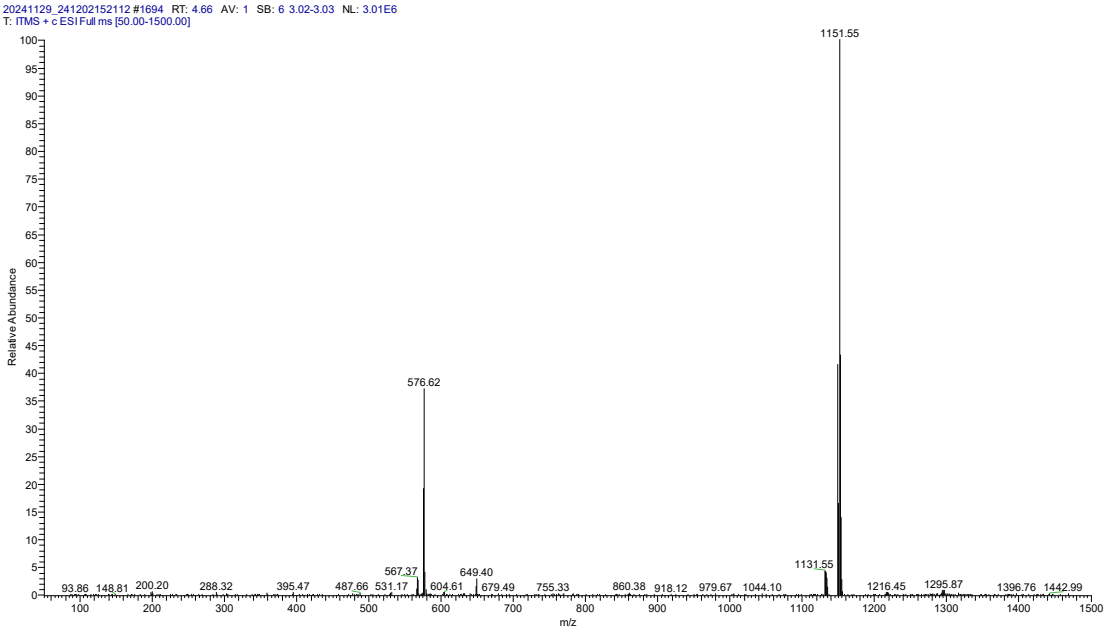

Figure S3. ESI-MS spectrum of **Ir3**.

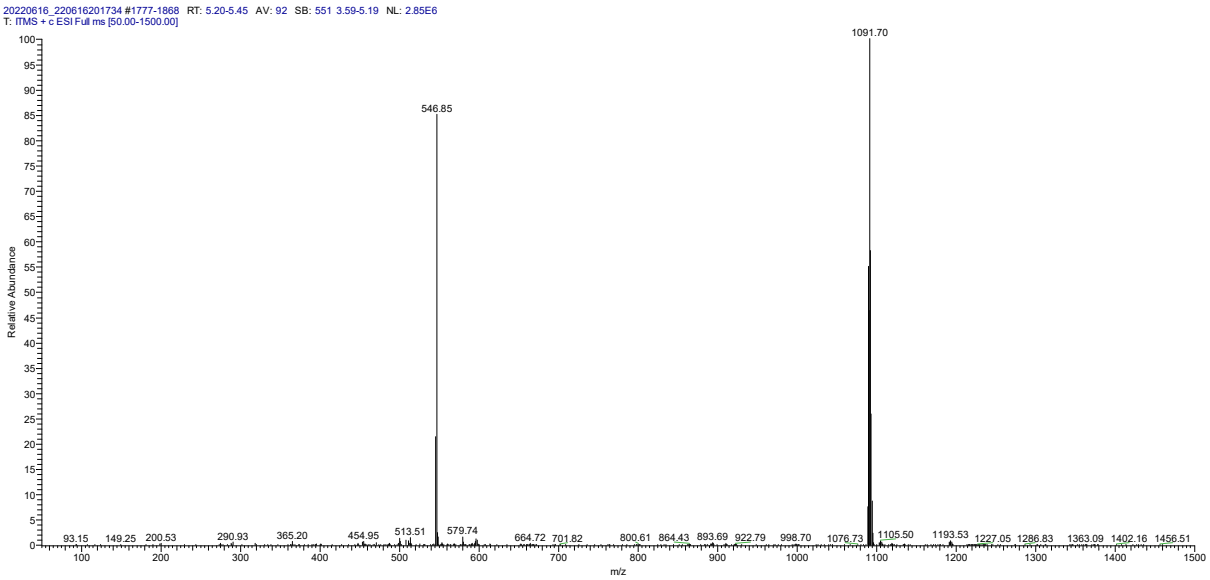

Figure S4. ESI-MS spectrum of **Ir4**.

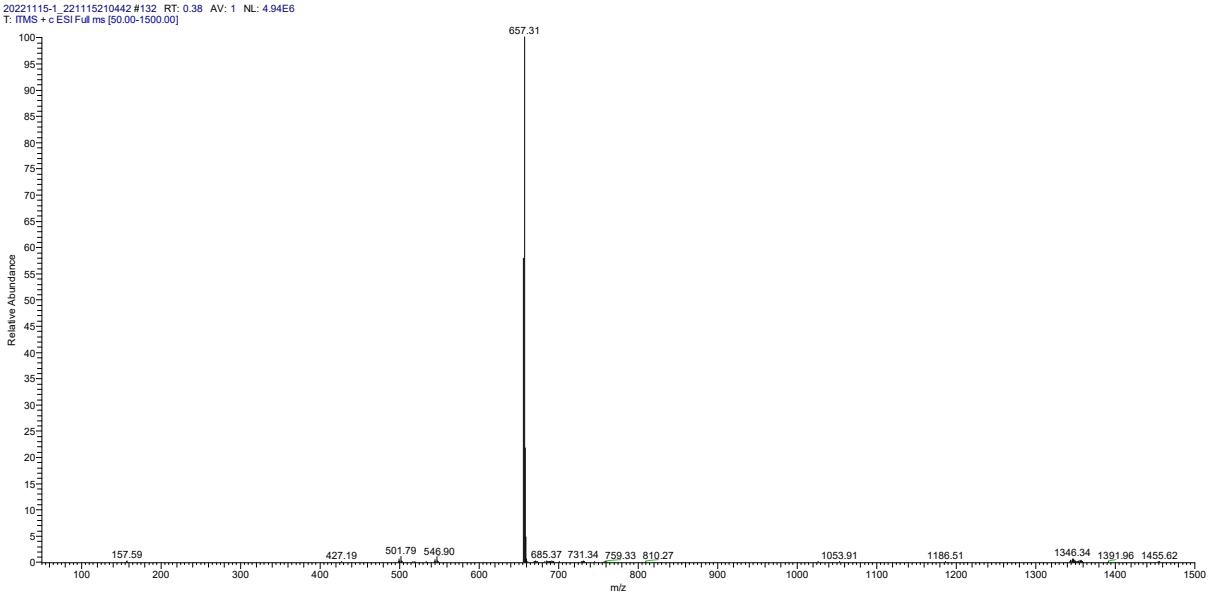

Figure S5. ESI-MS spectrum of **Ir1a**.

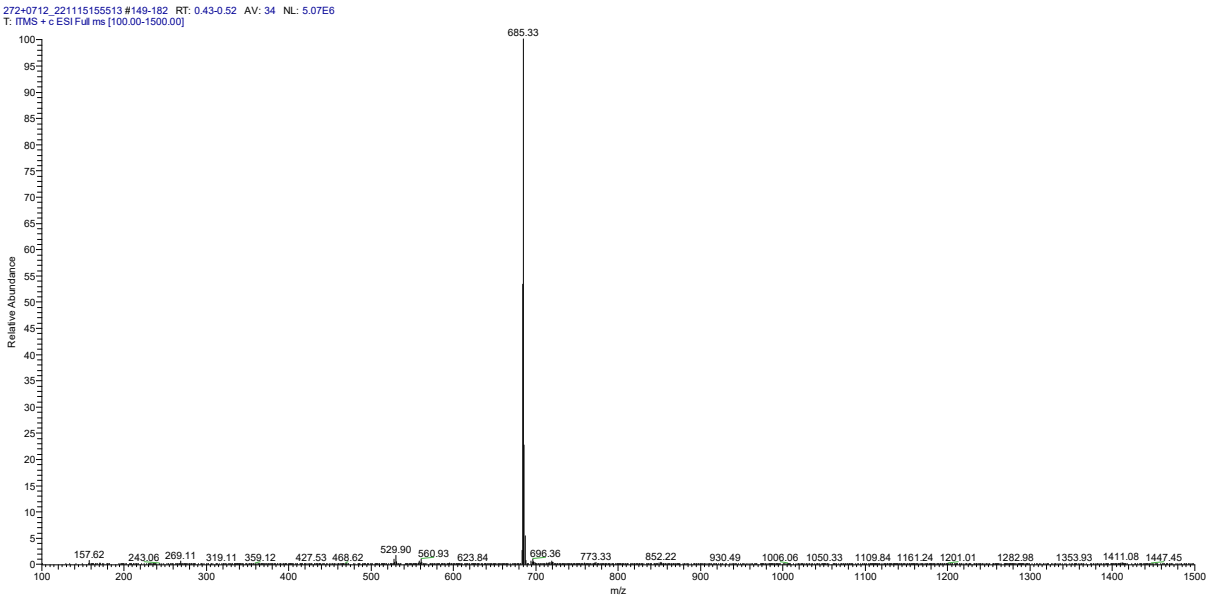

Figure S6. ESI-MS spectrum of **Ir2a**.

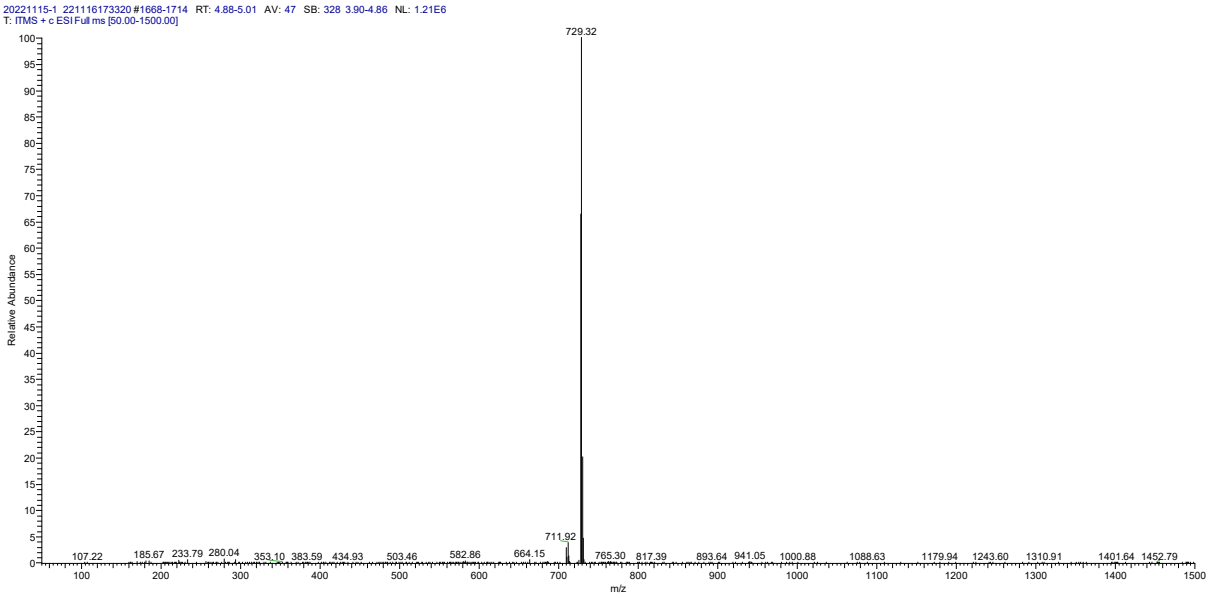

Figure S7. ESI-MS spectrum of **Ir3a**.

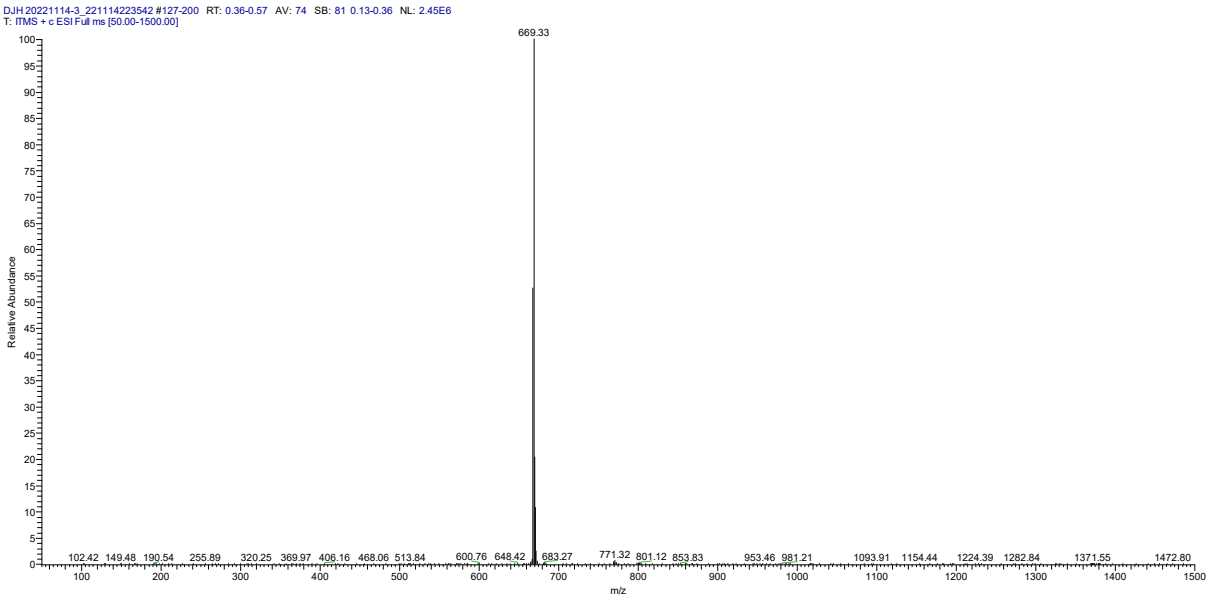

Figure S8. ESI-MS spectrum of **Ir4a**.

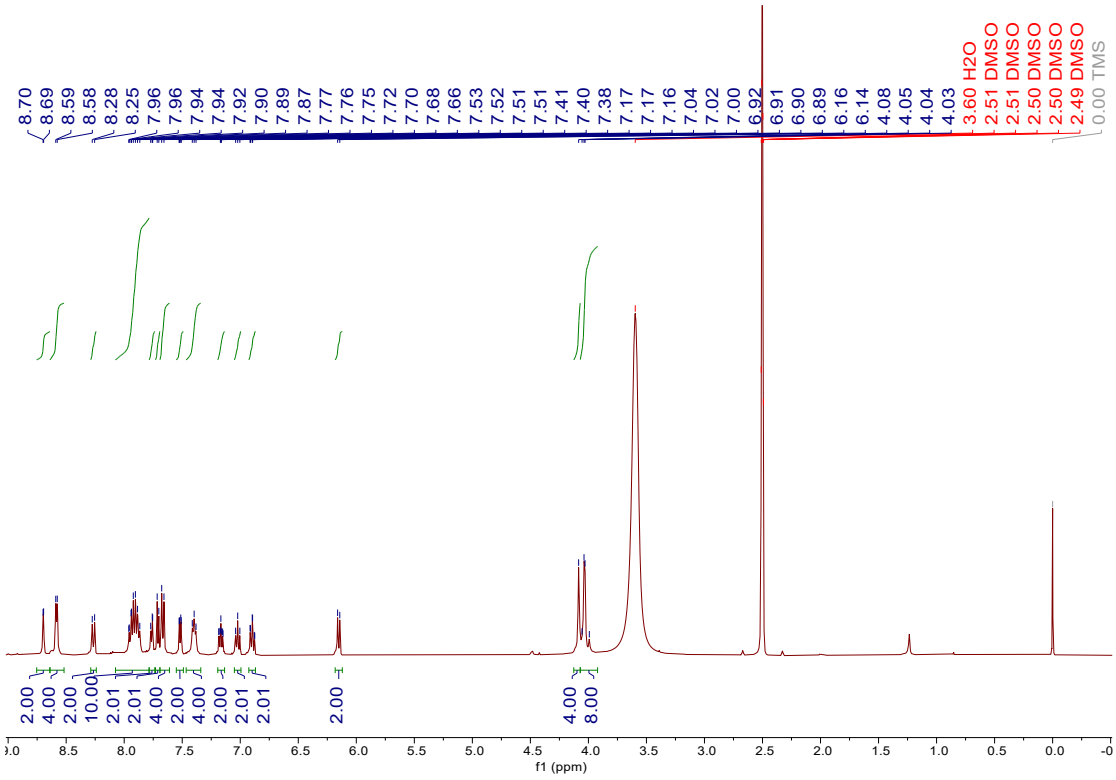

Figure S9. ^{1}H NMR of **Ir1** in DMSO-d_6.

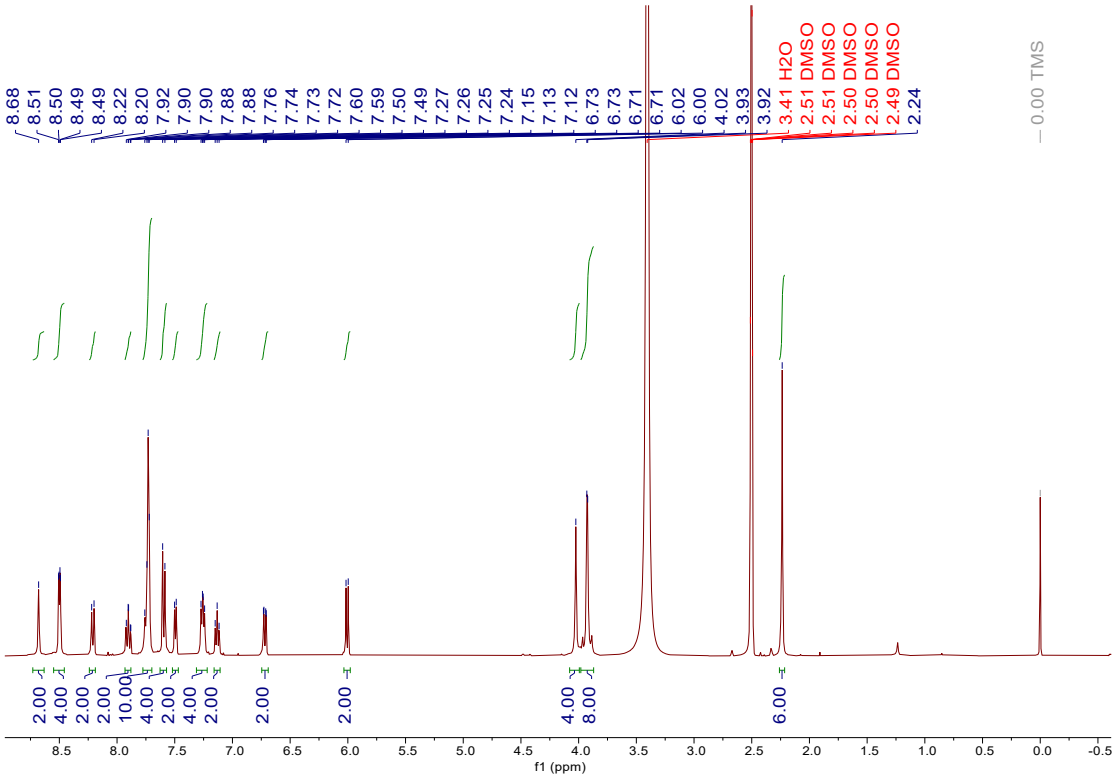

Figure S10. ^{1}H NMR of **Ir2** in DMSO-d_6.

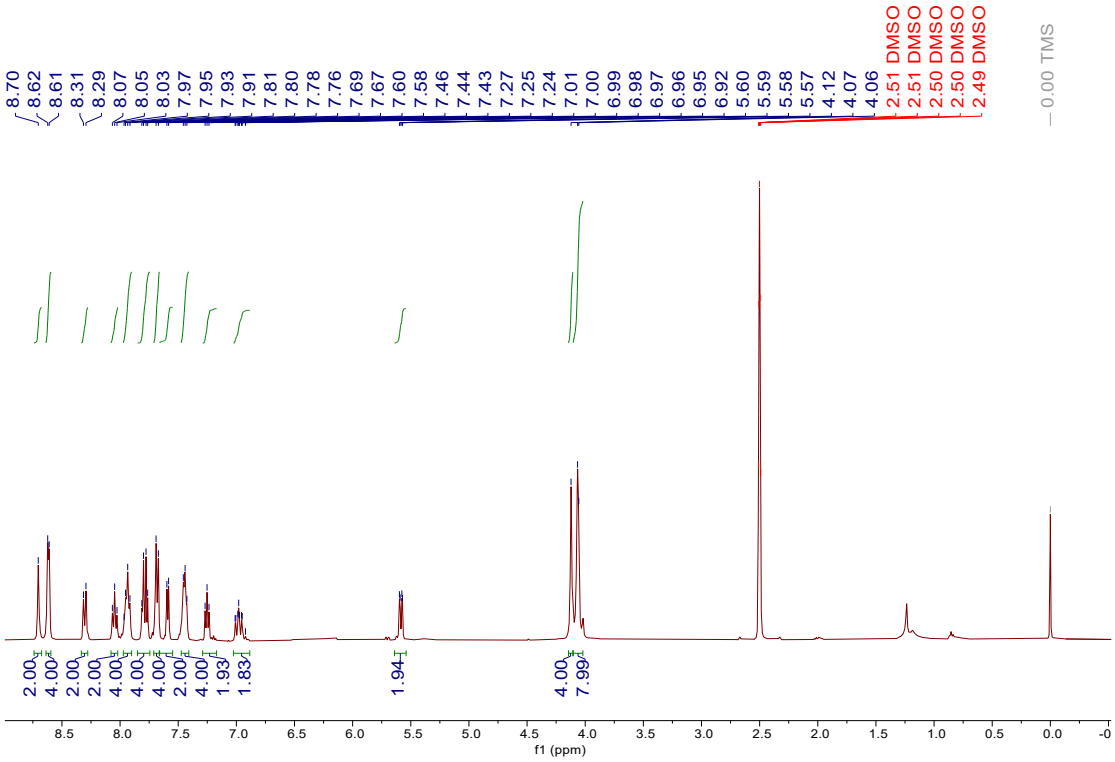

Figure S11. ^{1}H NMR of **Ir3** in DMSO-d_6.

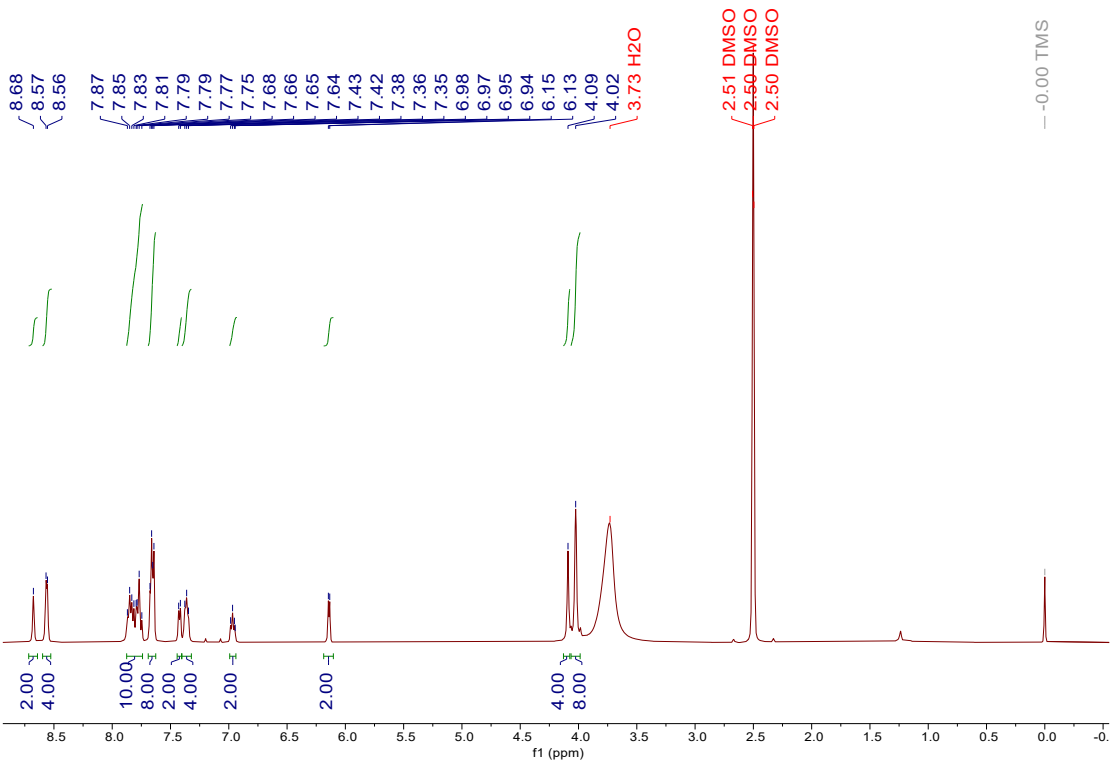

Figure S12. ^{1}H NMR of **Ir4** in DMSO-d_6.

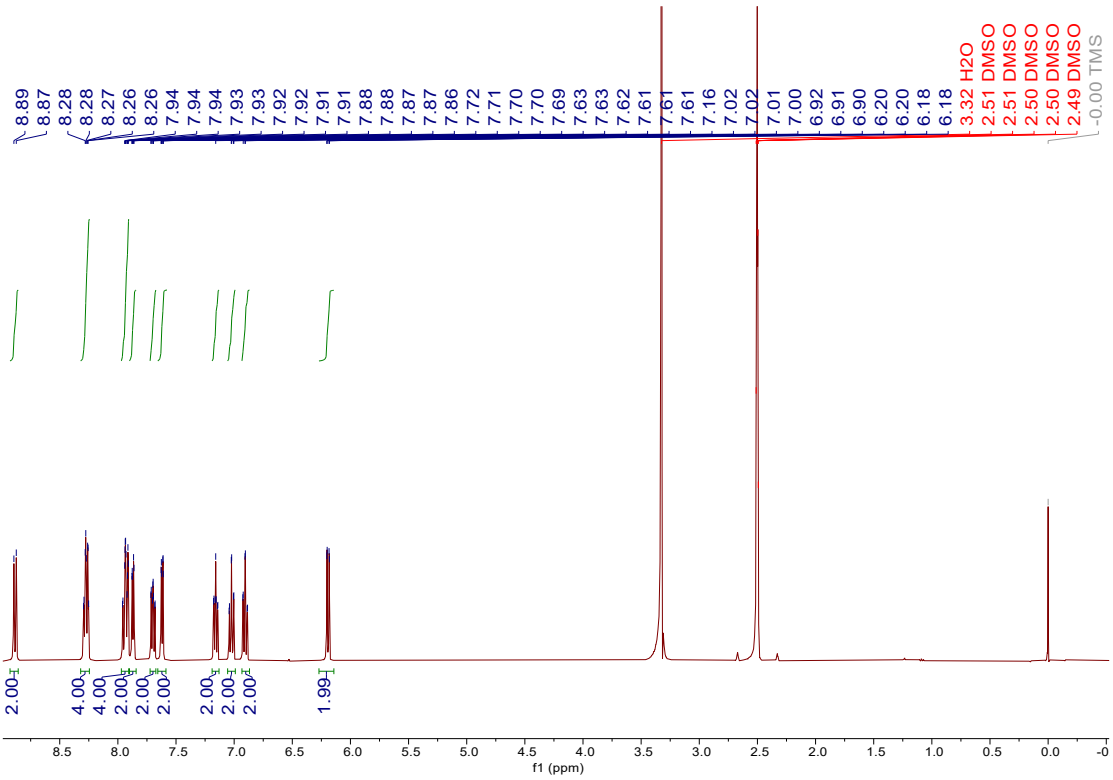

Figure S13. ^{1}H NMR of **Ir1a** in DMSO-d_6.

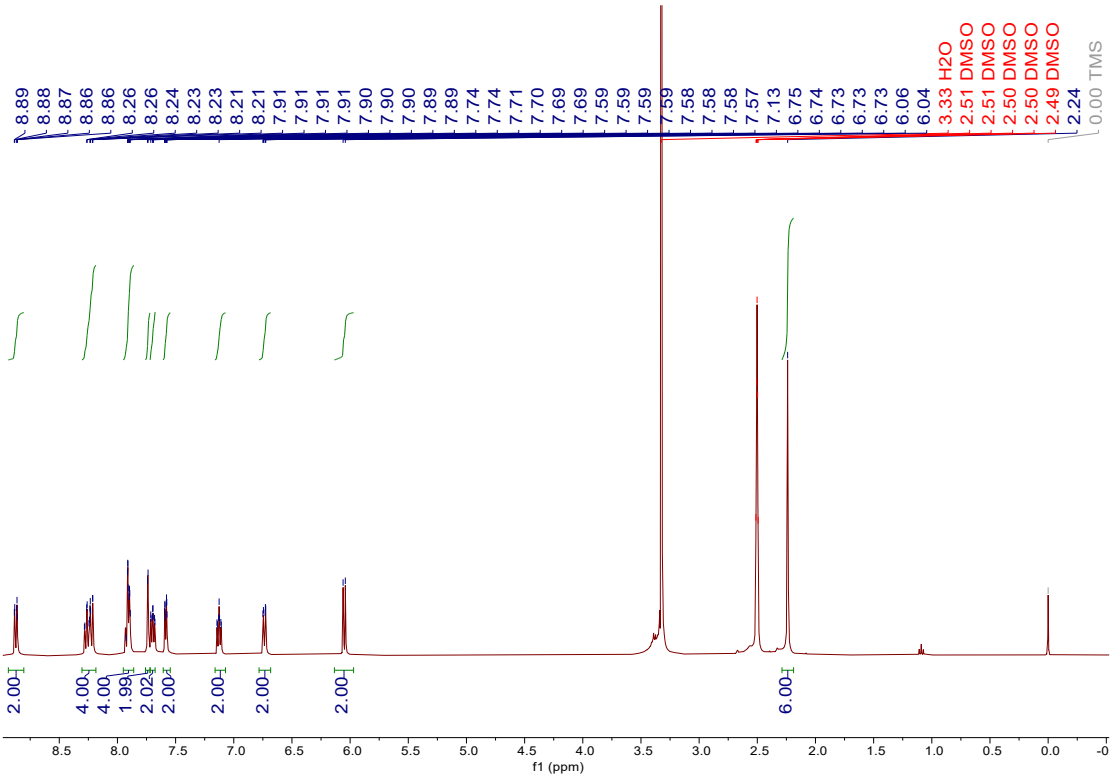

Figure S14. ^{1}H NMR of **Ir2a** in DMSO-d_6.

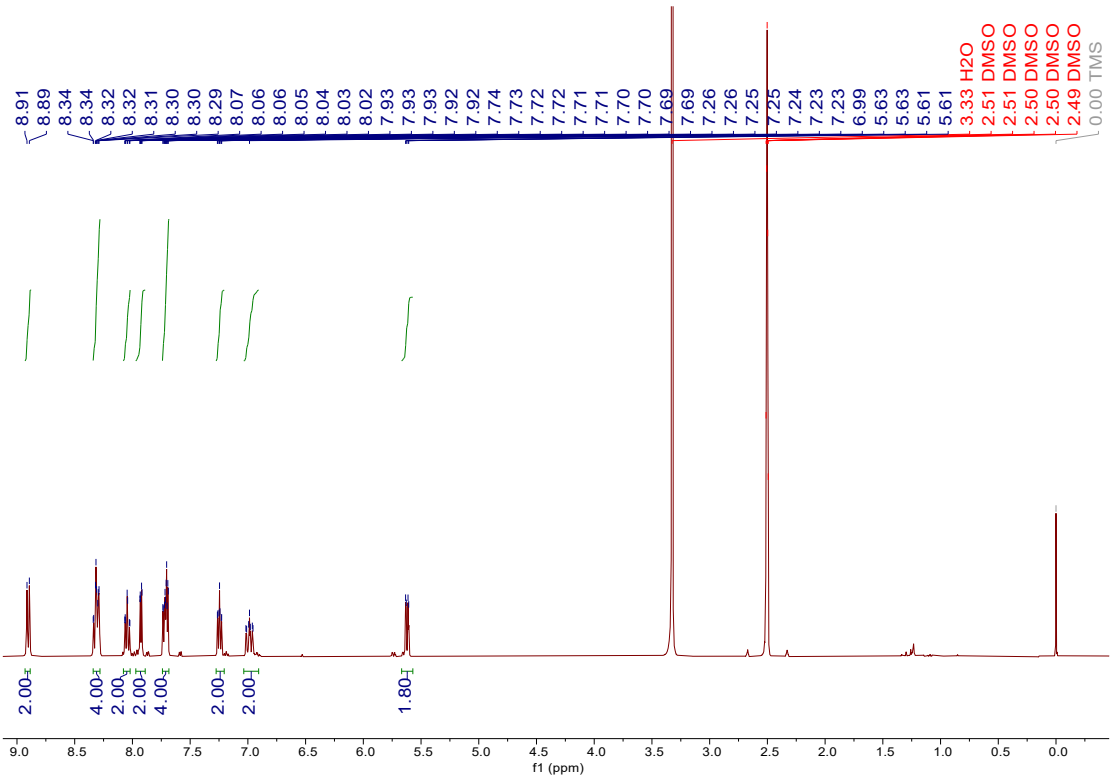

Figure S15. ^{1}H NMR of **Ir3a** in DMSO-d_6.

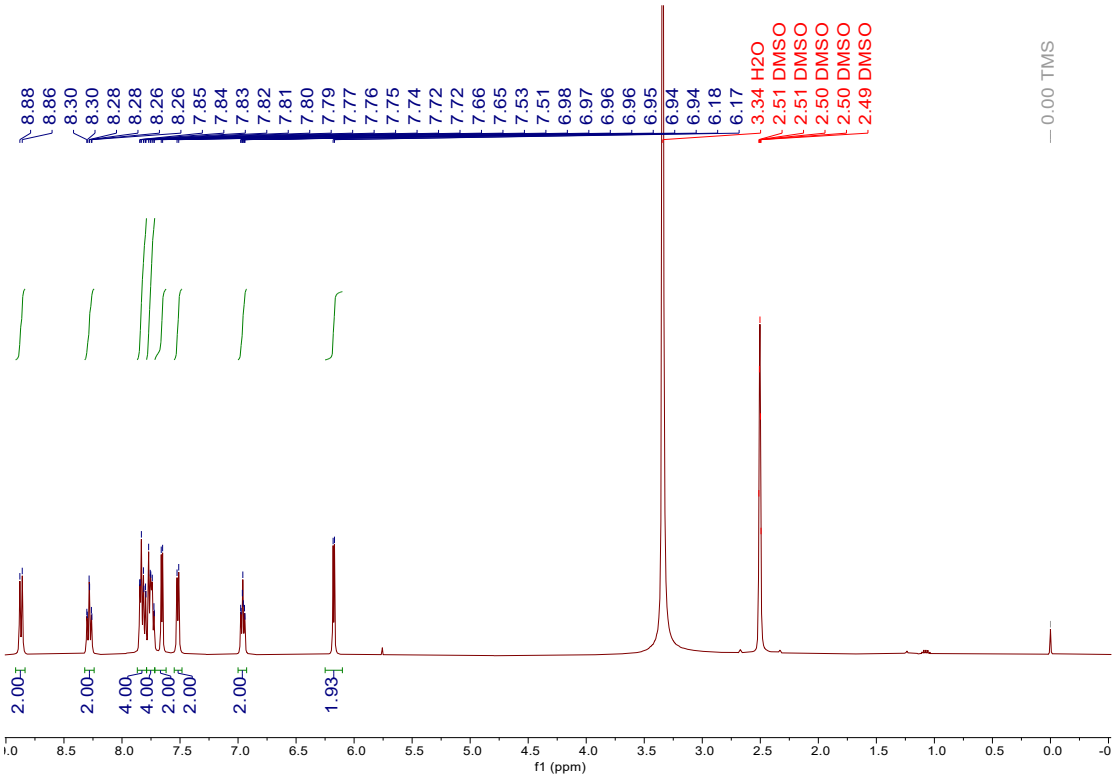

Figure S16. ^{1}H NMR of **Ir4a** in DMSO-d_6.

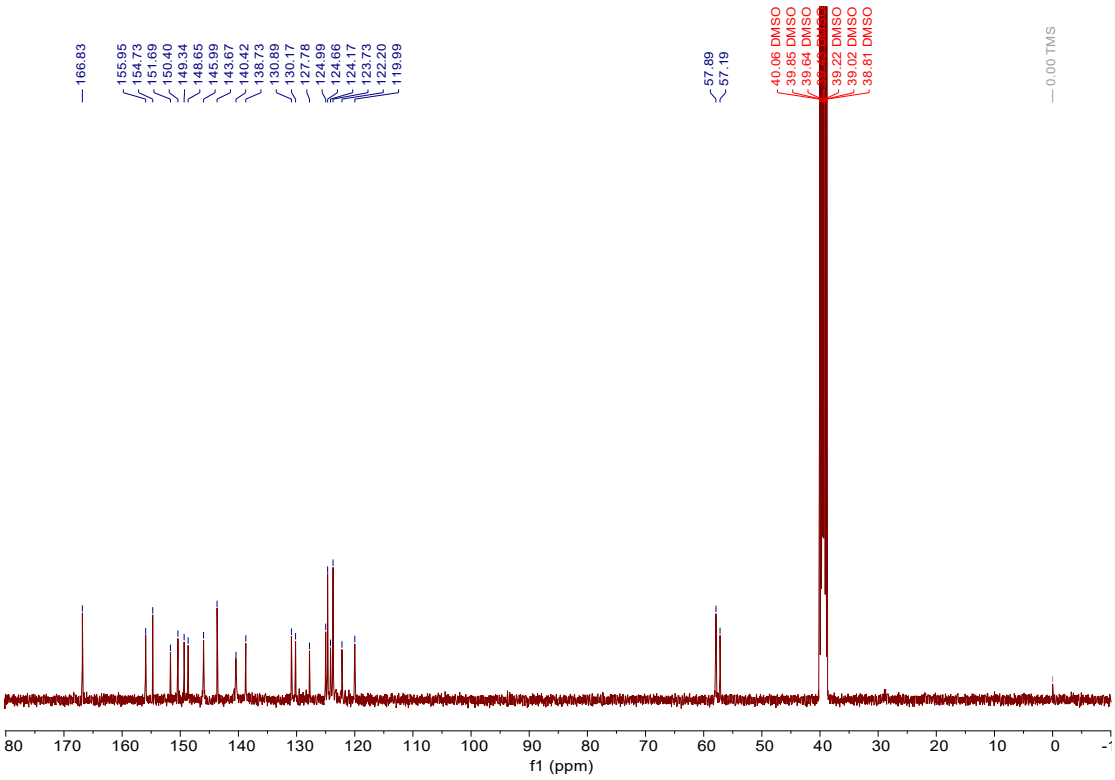

Figure S17. ^{13}C NMR of **Ir1** in DMSO-d_6.

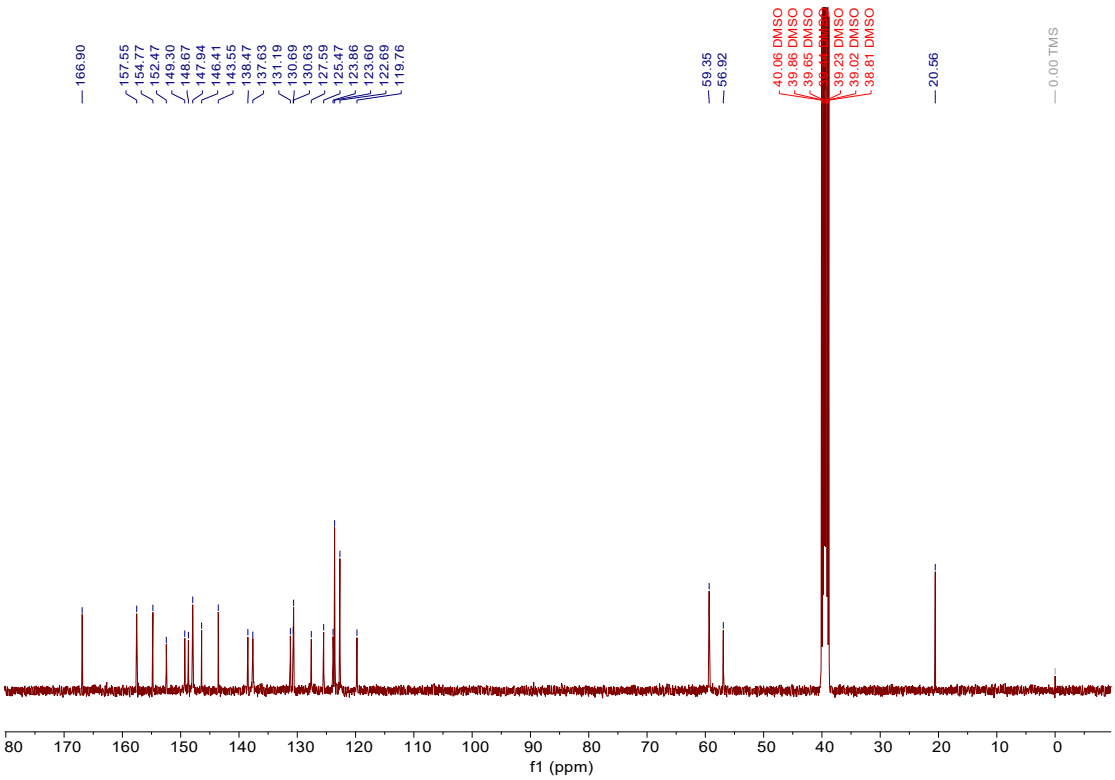

Figure S18. ^{13}C NMR of **Ir2** in DMSO-d_6.

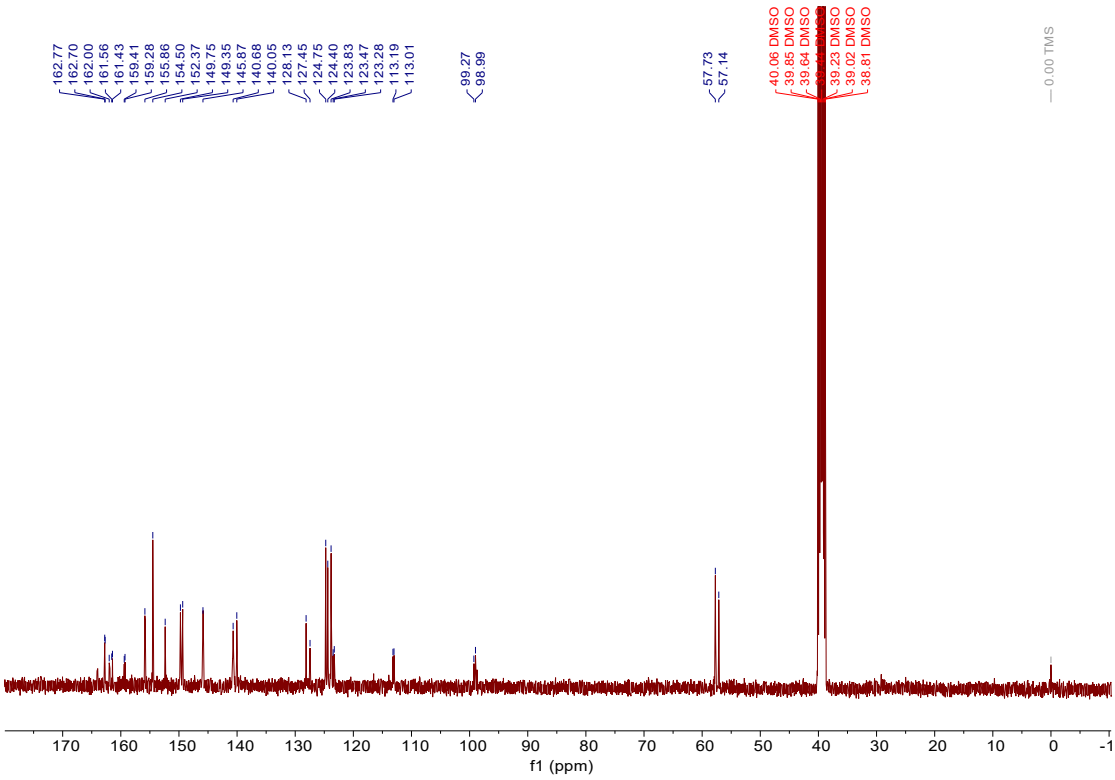

Figure S19. ^{13}C NMR of **Ir3** in DMSO-d_6.

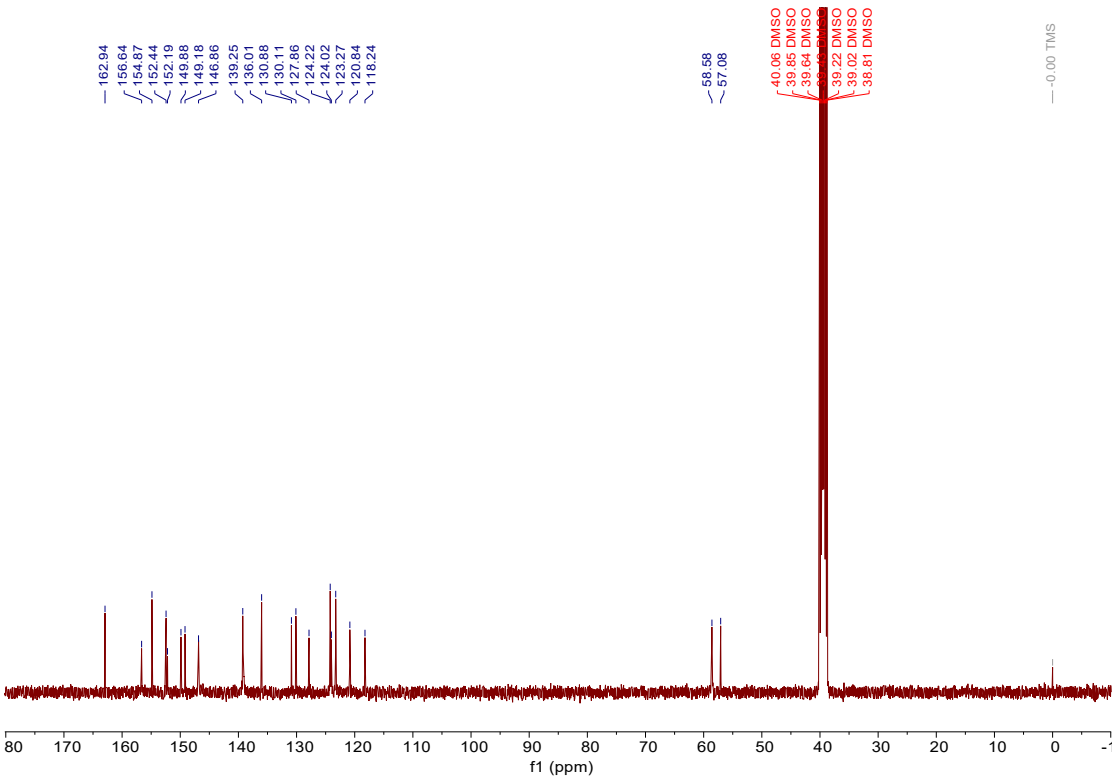

Figure S20. ^{13}C NMR of **Ir4** in DMSO-d_6.

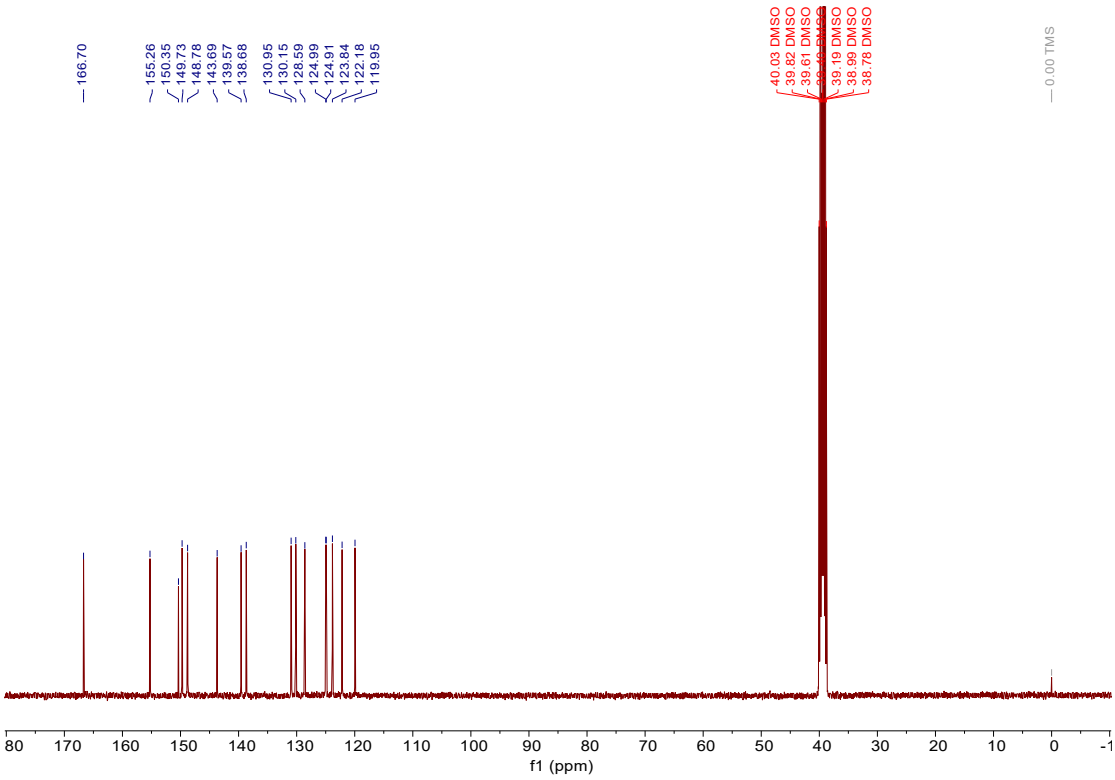

Figure S21. ^{13}C NMR of **Ir1a** in DMSO-d_6.

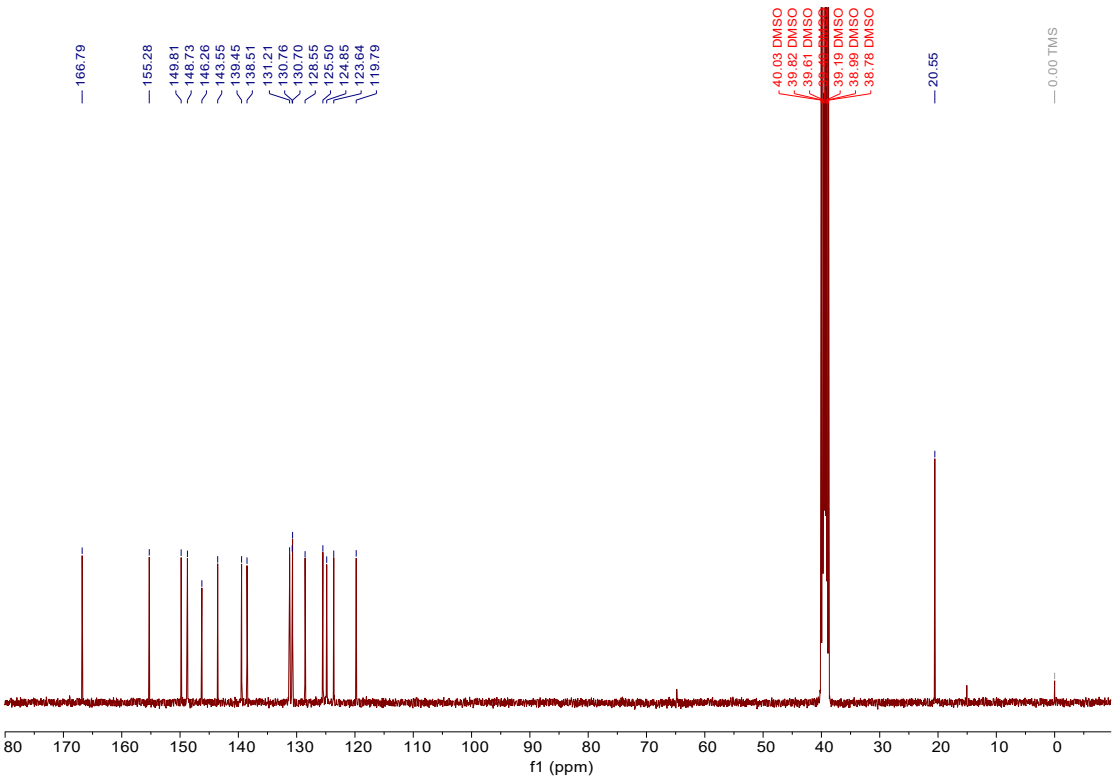

Figure S22. ^{13}C NMR of **Ir2a** in DMSO-d_6.

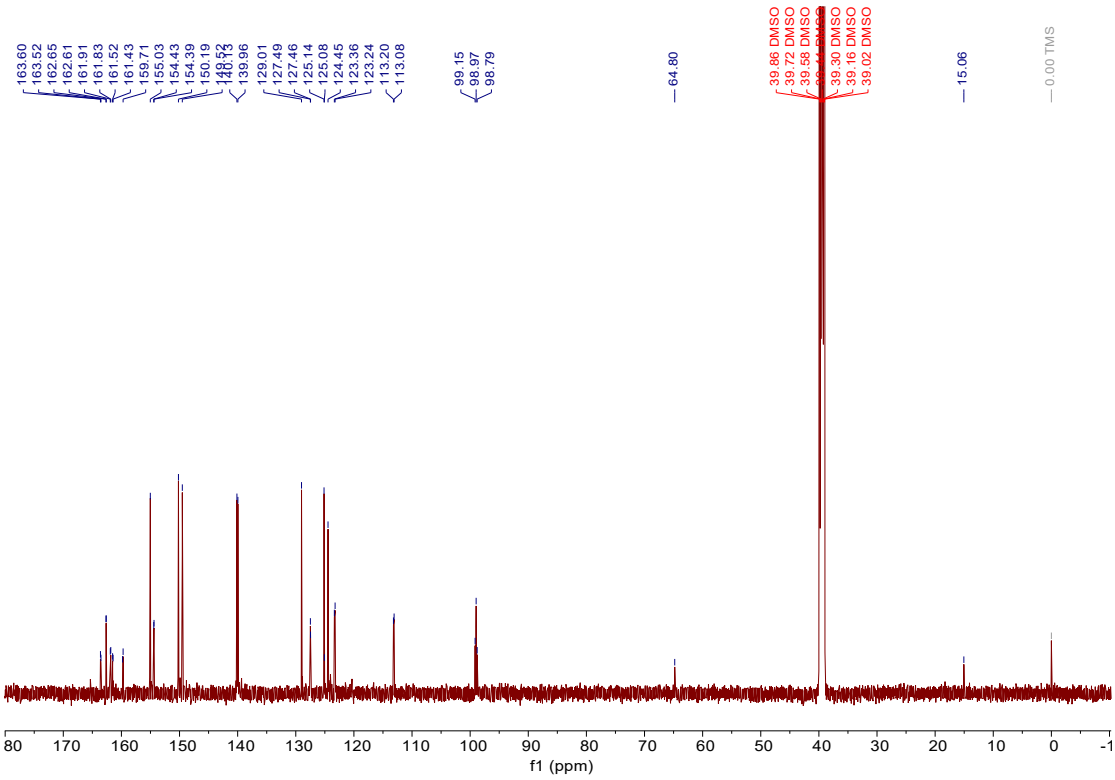

Figure S23. ^{13}C NMR of **Ir3a** in DMSO-d_6.

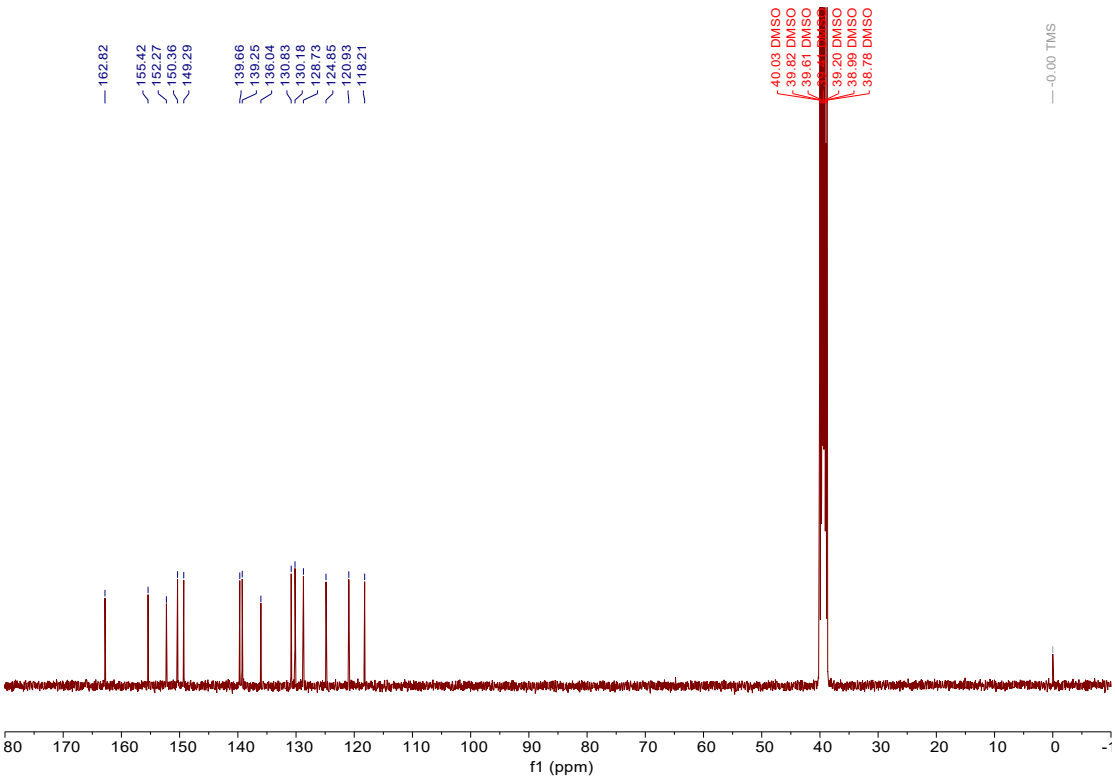

Figure S24. ^{13}C NMR of **Ir4a** in DMSO-d_6.

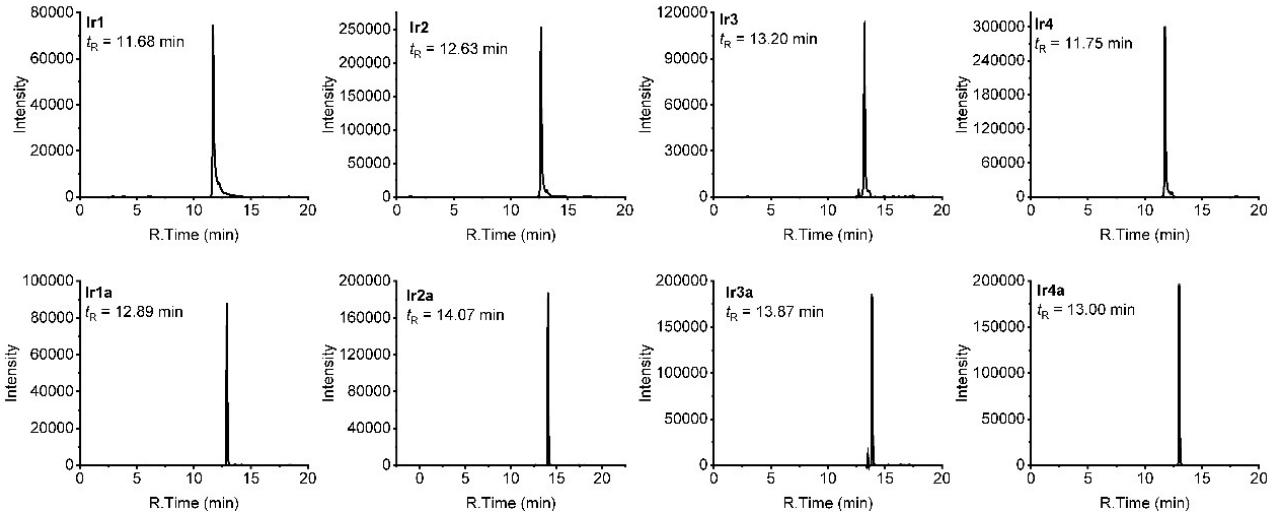

Figure S25. Purity of Ir(III) complexes analyzed by HPLC.

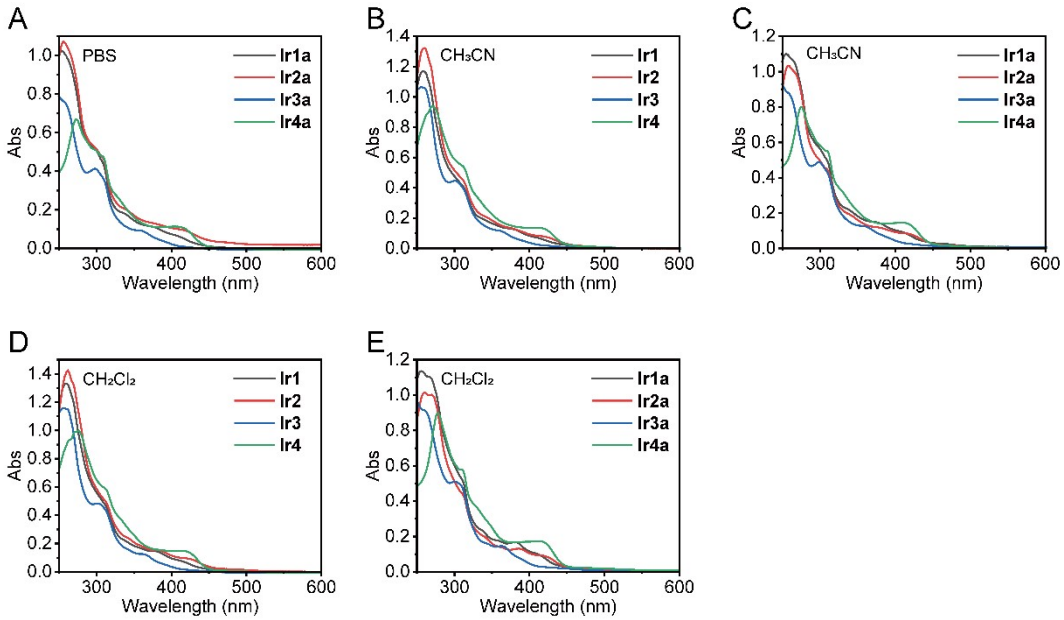

Figure S26. UV-Vis absorption spectra the Ir(III) complexes (20.0 μM) in different solvents.

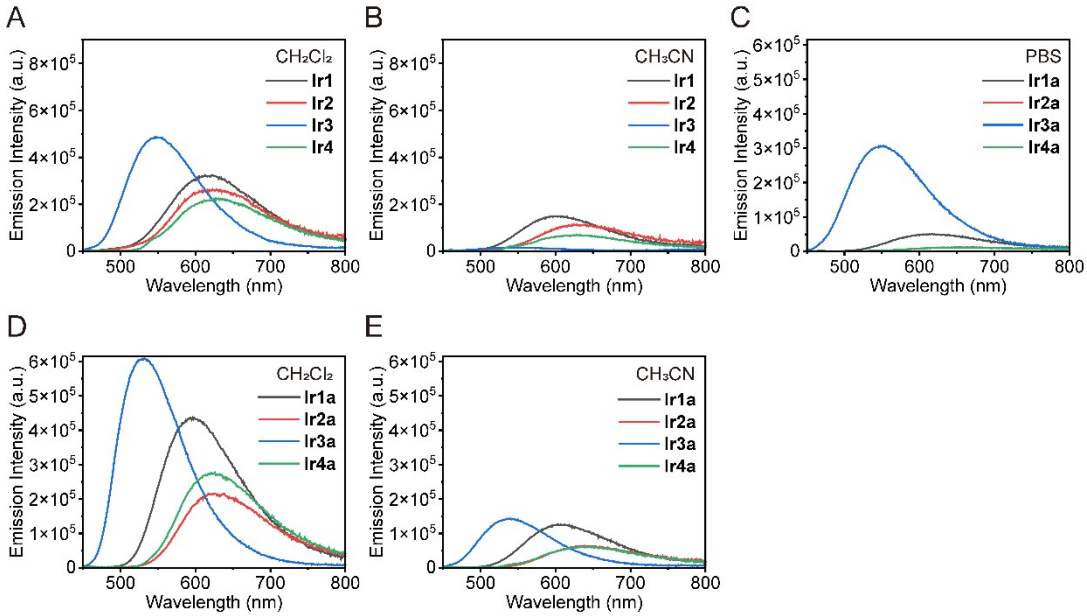

Figure S27. Emission spectra the Ir(III) complexes (20.0 μM) in different solvents.

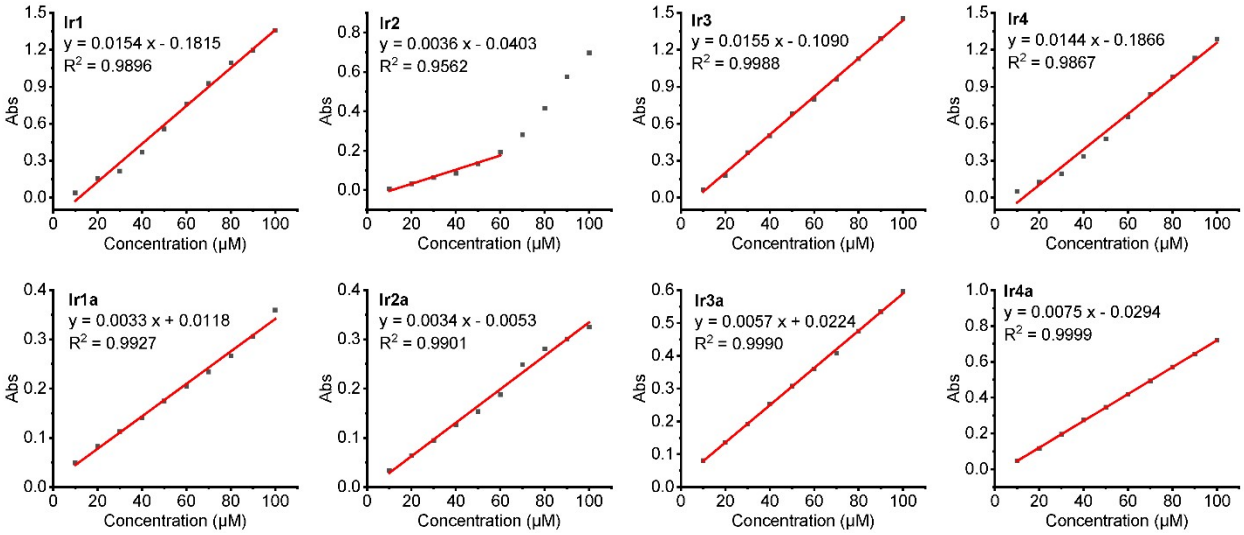

Figure S28. Fitting curves of the absorbance of Ir(III) complexes at maximum absorption wavelength ($\lambda_{abs,max}$) vs concentration, respectively. Ir(III) complexes were dissolved in degassed PBS and 1% DMSO (v/v) was used for solubilization.

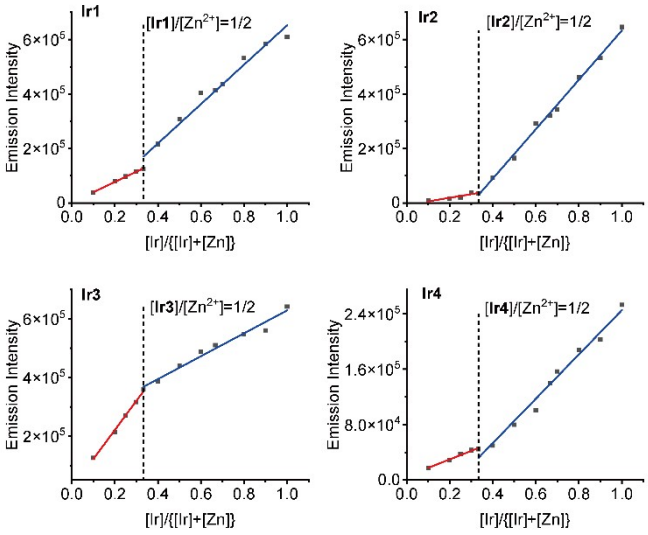

Figure S29. The Job's plot of **Ir1–Ir4** with varying mole fractions of Zn^{2+}. Total concentration was kept to 30 μM.

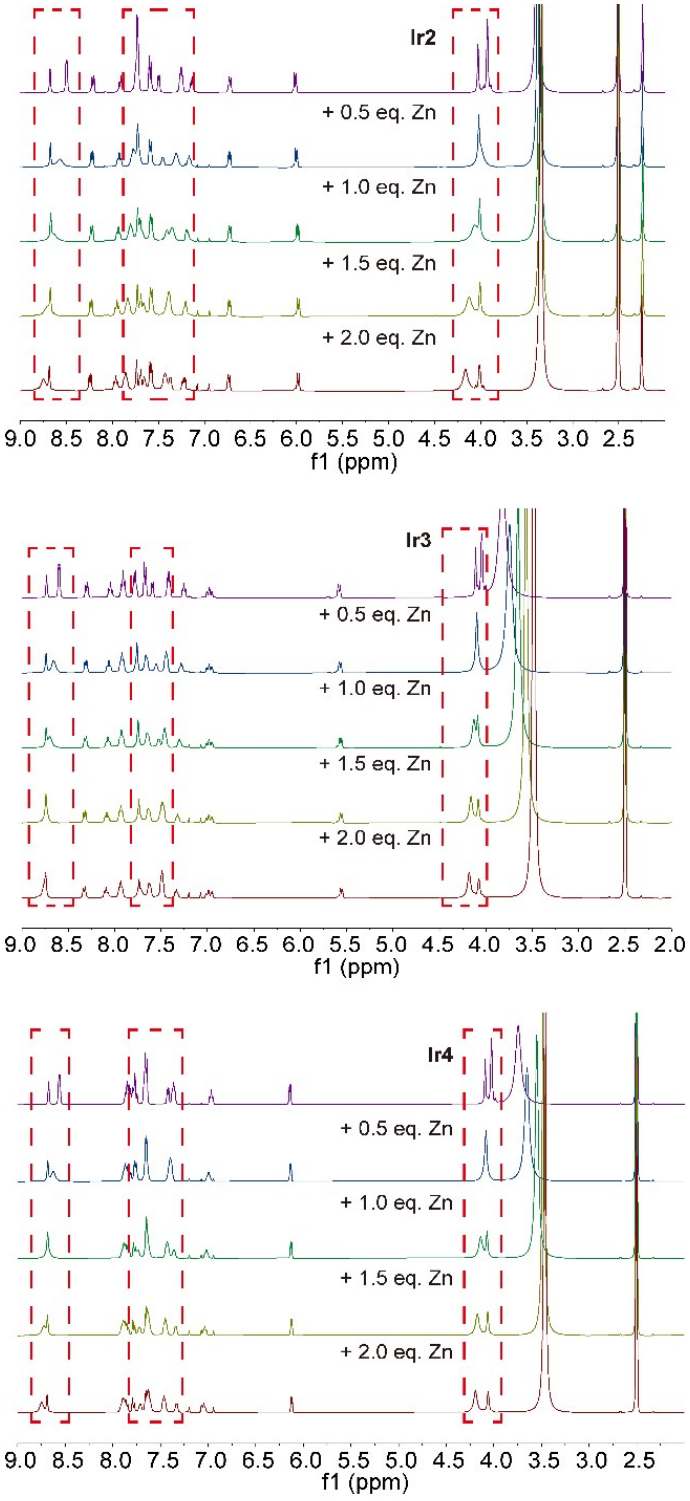

Figure S30. ^{1}H NMR spectra of **Ir2–Ir4** titrated with 0–2.0 equiv. Zn^{2+} in d^{6}-DMSO/H_2O.

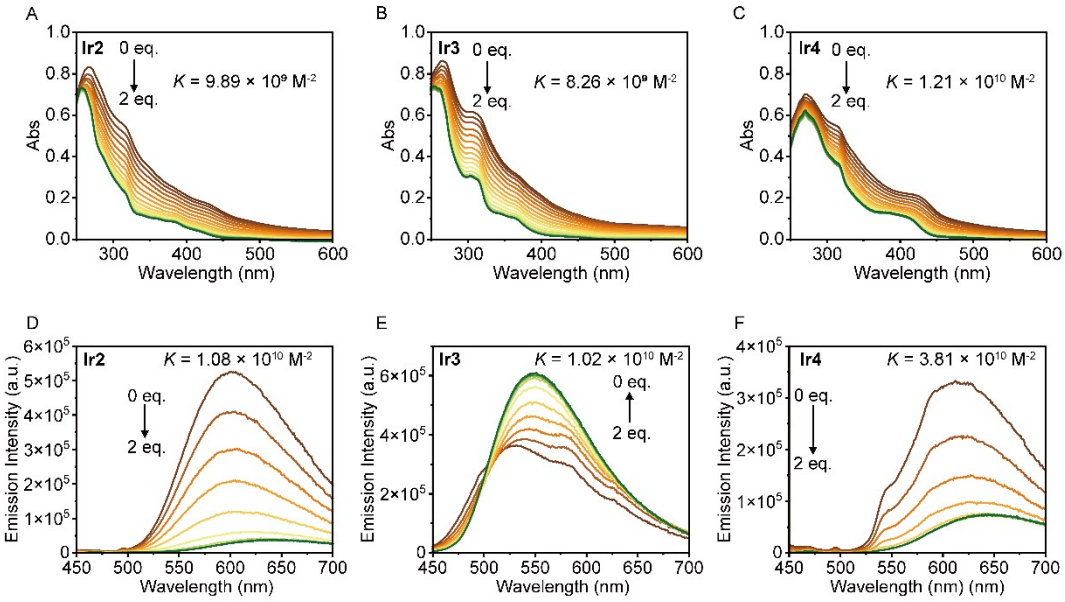

Figure S31. (A-C) The UV/Vis titration plots of **Ir2–Ir4** (20.0 μM) with Zn^{2+} (0–2.0 equiv.) in degassed PBS. (D-F) The emission titration plots of **Ir2–Ir4** (20.0 μM) with Zn^{2+} (0–2.0 equiv.) in degassed PBS. The binding constants (*K*) were obtained by dividing the intercept by the slope of the fitted plots shown in Figure S30.

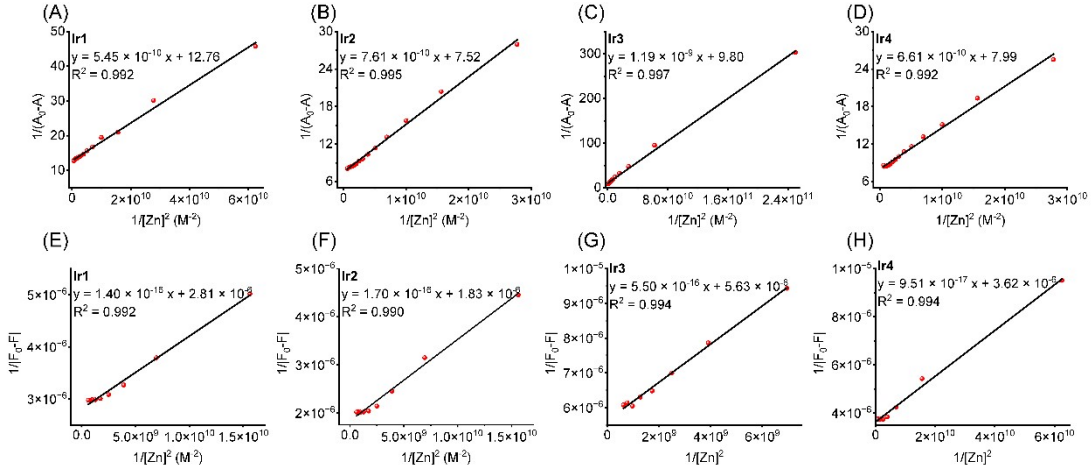

Figure S32. (A-D) The fitted plots of UV/Vis titration of **Ir1–Ir4** with Zn^{2+}. (E-H) The fitted plots of emission titration of **Ir1–Ir4** with Zn^{2+}. The binding constants (*K*) were obtained by dividing the intercept by the slope.

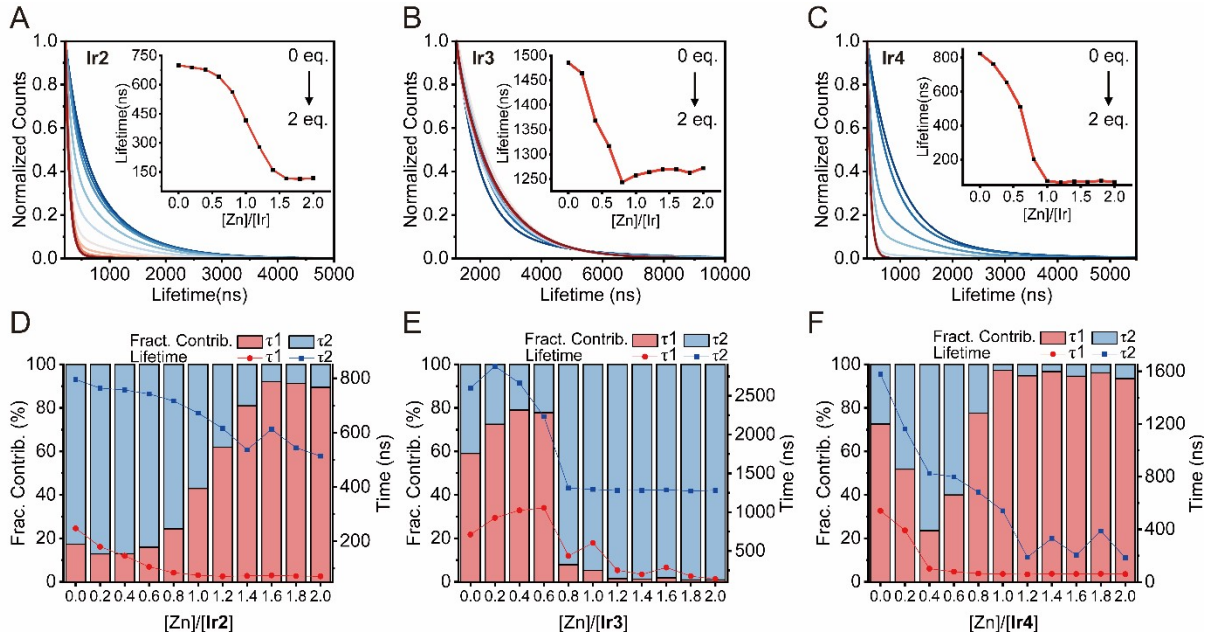

Figure S33. Phosphorescence decay traces (A-C), the corresponding numerical lifetimes and fractional contribution values (D–F) of **Ir2**–**Ir4** (20 μM) upon titration with Zn^{2+} (0–2.0 equiv.) in degassed PBS. Inset: plots of phosphorescence lifetimes varies with the ratios of Ir(III) to Zn^{2+}.

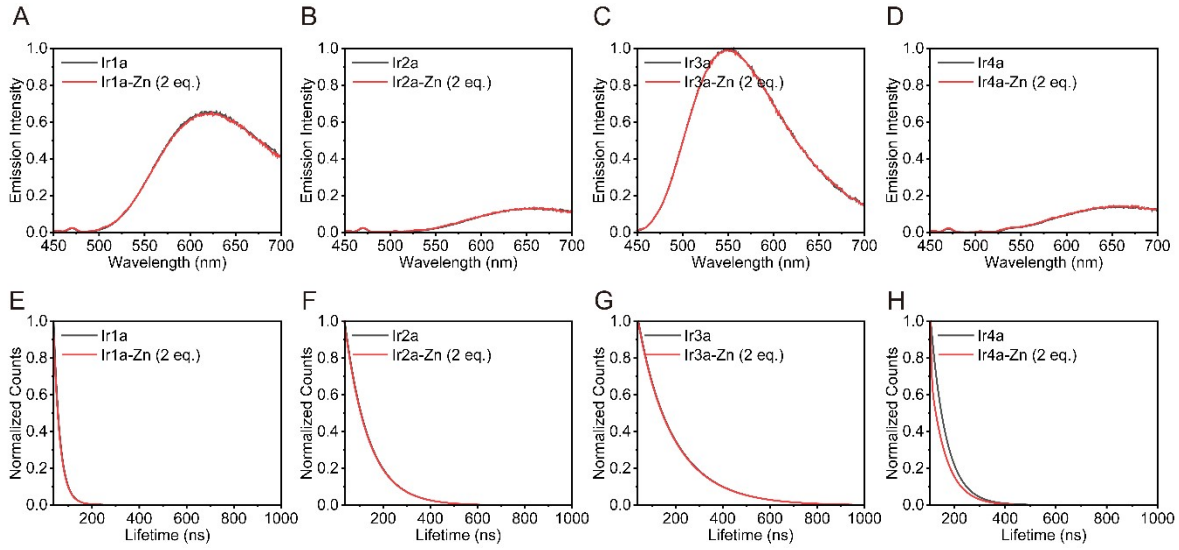

Figure S34. The normalized emission spectra and emission decay curves of **Ir1a**–**Ir4a** (20.0 μM) in the absence and presence of Zn^{2+} (2.0 equiv.) in degassed PBS.

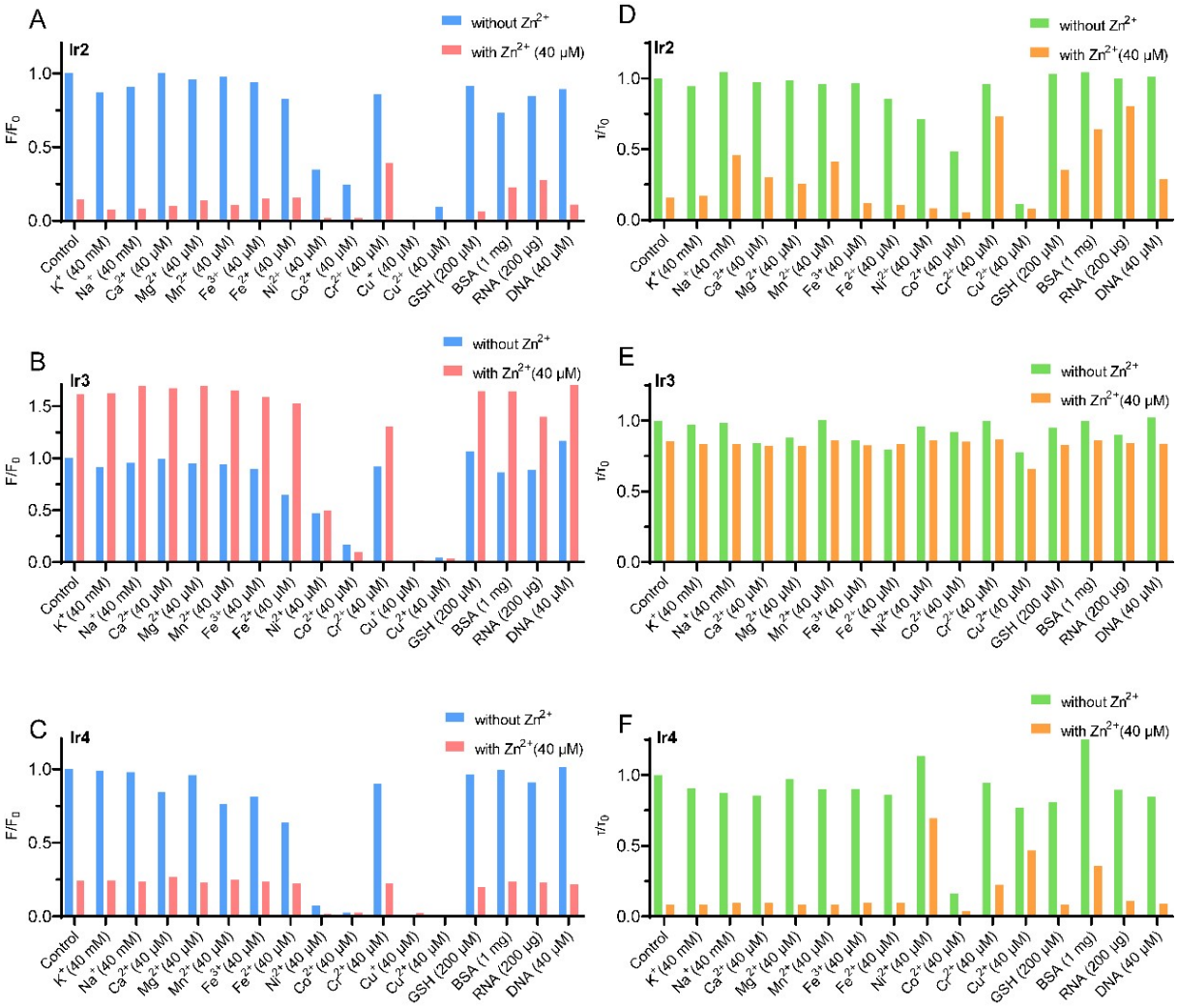

Figure S35. (A-C) Histogram of fluorescence intensity ratios of **Ir2–Ir4** (20 μM) in 2 mL PBS under different states. (D-F) Histogram of fluorescence lifetime ratios of **Ir2–Ir4** (20 μM) in 2 mL PBS under different states. λ_{ex} = 405 nm.

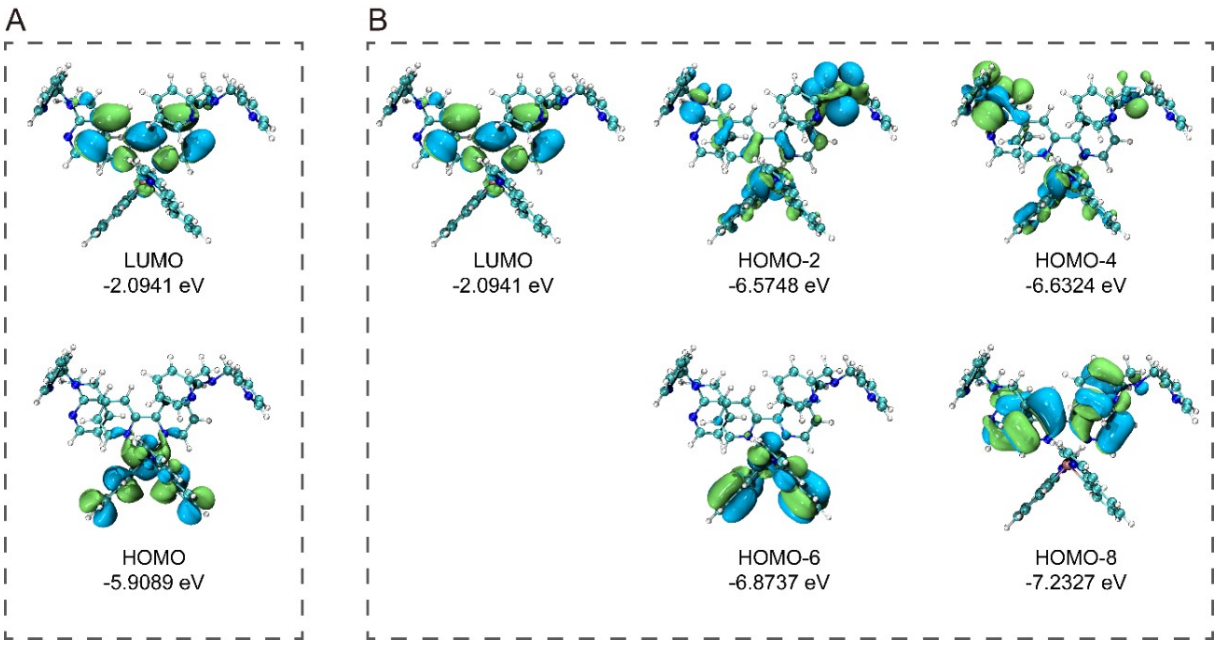

Figure S36. DFT-calculated frontier molecular orbitals involved in T_1 (A) and T_2 (B) for **Ir1**.

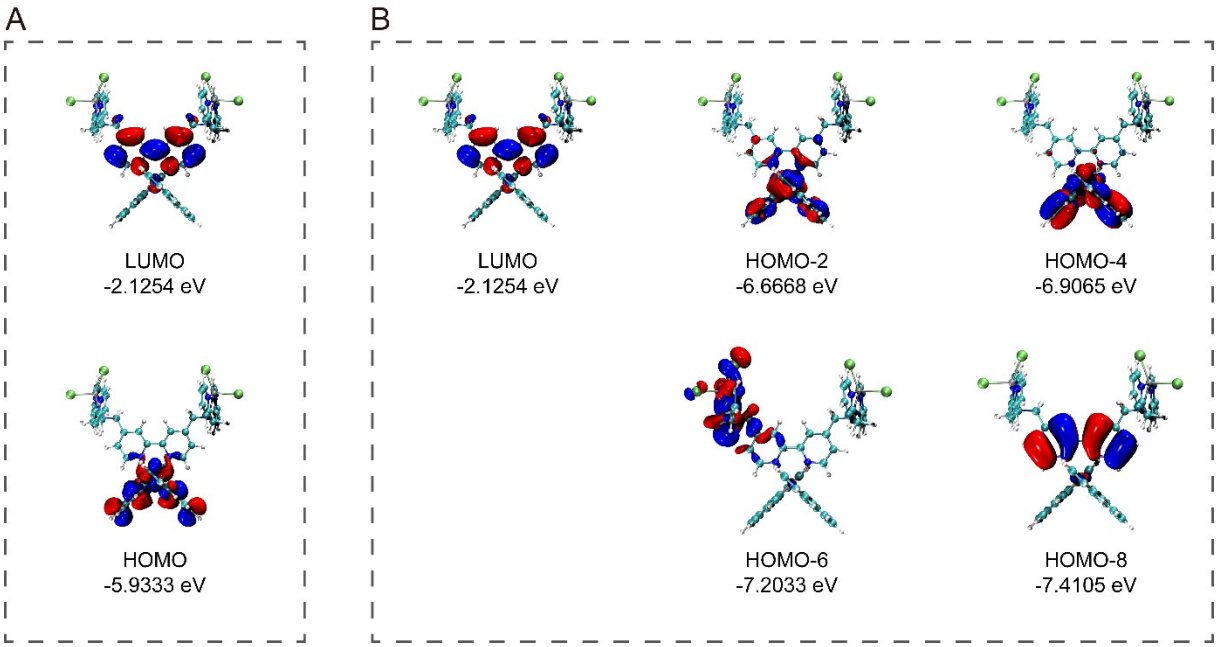

Figure S37. DFT-calculated frontier molecular orbitals involved in T_1 (A) and T_2 (B) for **Ir1-Zn**.

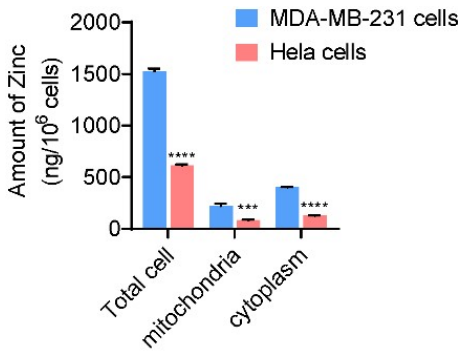

Figure S38. Cellular zinc contents of MDA-MB-231 cells and Hela cells measured by ICP-MS. The data are presented as the means ± SD of three independent experiments. $^{***}p < 0.001$, $^{****}p < 0.0001$, compared with the control group.

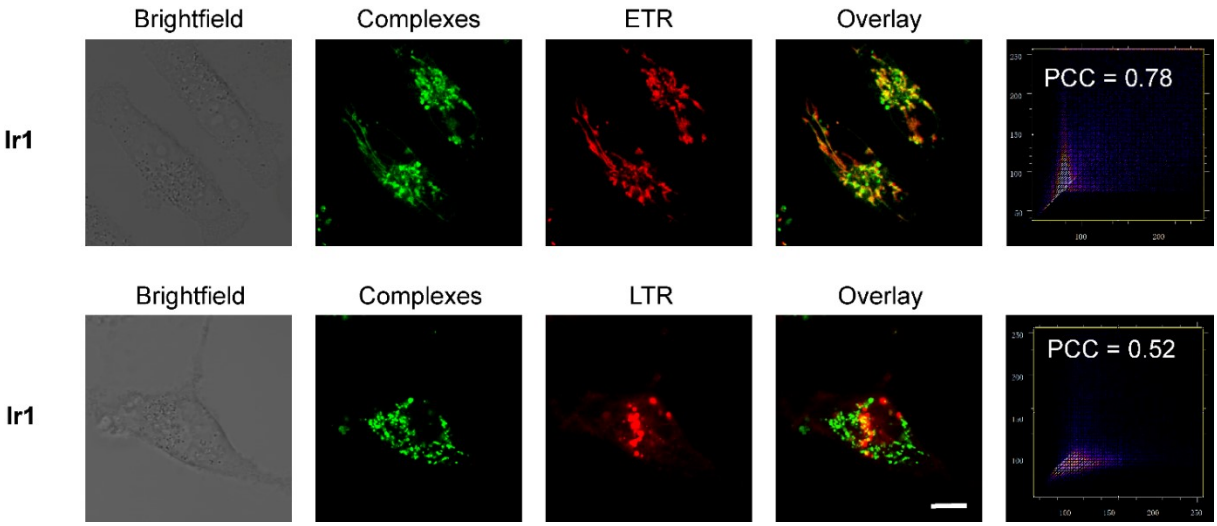

Figure S39. Colocalization images of **Ir1** with ETR and LTDR in MDA-MB-231 cells. Cells were treated with **Ir1** (2 μM, 60 min) and then incubated with ETR (1 μM, 15 min) or LTR (1 μM, 15 min). **Ir1**: λ_{ex} = 405 nm; λ_{em}= 600 ± 20 nm. ETR: λ_{ex} = 561 nm. λ_{em} = 615 ± 20 nm. LTR: λ_{ex} = 561 nm. λ_{em} = 615 ± 20 nm. Scale bar: 10.0 μm.

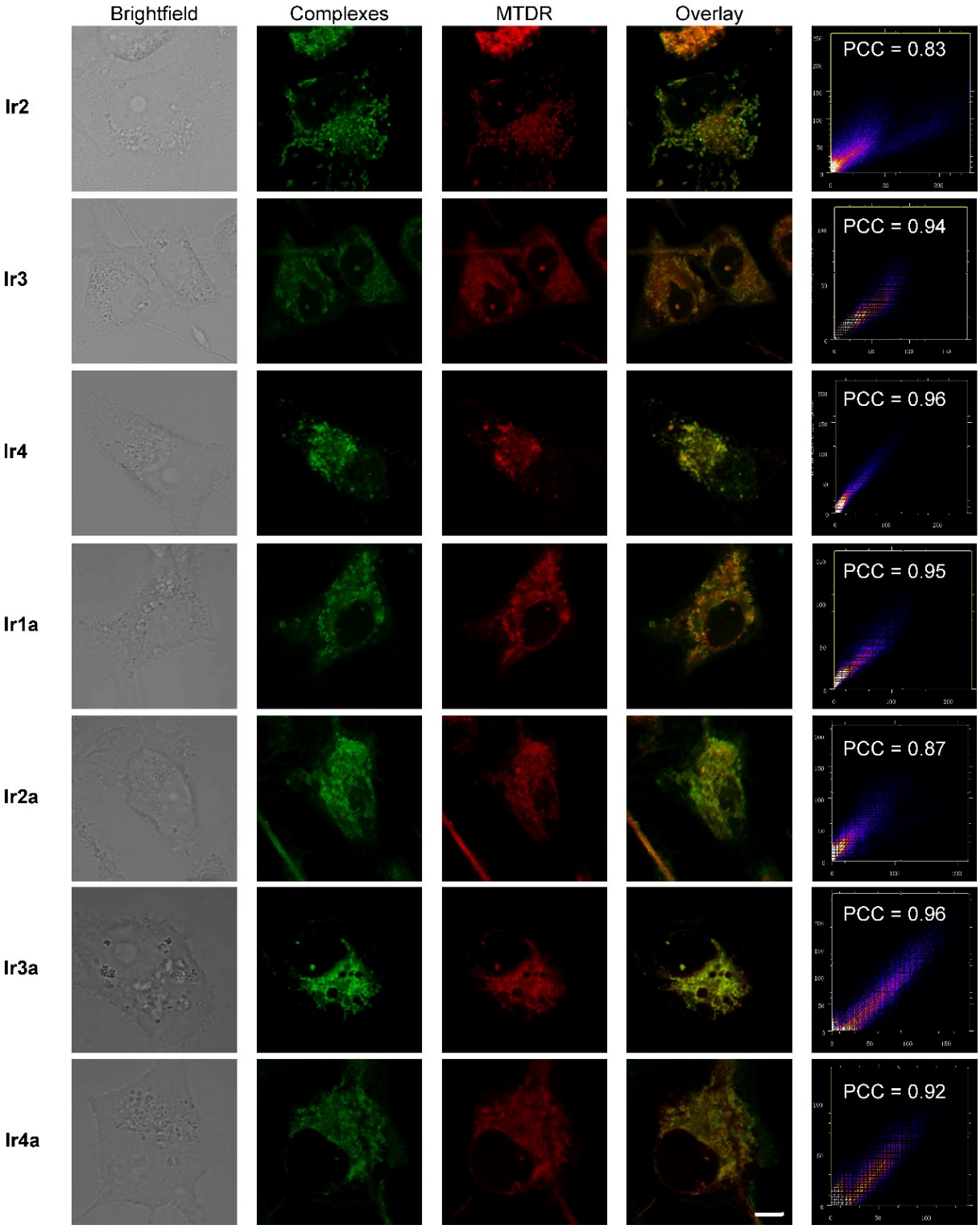

Figure S40. Colocalization images of **Ir2**–**Ir4** and **Ir1a**–**Ir4a** with MTDR in MDA-MB-231 cells. Cells were treated with **Ir2**–**Ir4** and **Ir1a**–**Ir4a** (2 µM, 60 min) and then incubated with MTDR (100 nM, 15 min). **Ir2**–**Ir4** and **Ir1a**–**Ir4a**: λ_{ex} = 405 nm; λ_{em}= 600 ± 20 nm. MTDR: λ_{ex} = 633 nm. λ_{em} = 660 ± 10 nm. Scale bar: 10.0 µm.

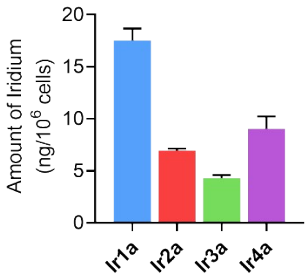

Figure S41. Cellular iridium contents measured by ICP-MS. MDA-MB-231 cells were treated with **Ir1a–Ir4a** (2 μM) for 1 h. The data are presented as the means ± SD of three independent experiments.

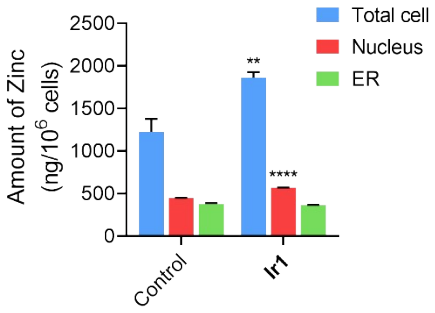

Figure S42. Cellular zinc contents measured by ICP-MS. MDB-MA-231 cells were treated with **Ir1** (2 μM) for 1 h. The data are presented as the means ± SD of three independent experiments. $^{**}p < 0.01$, $^{****}p < 0.0001$, compared with the control group.

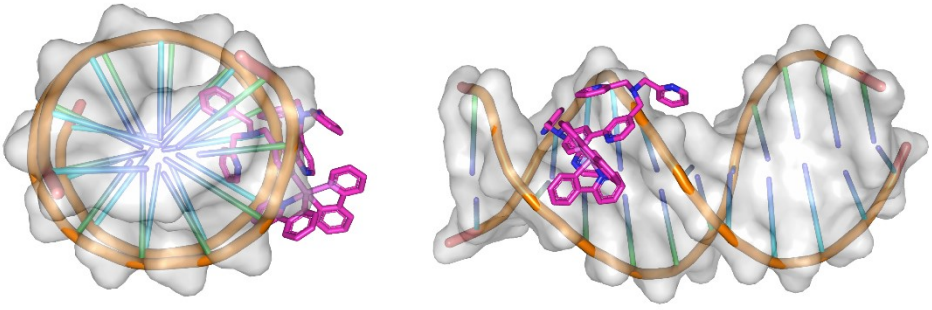

Figure S43. Molecular docking studies of **Ir1** with ds-DNA (PDB: 5t4w).

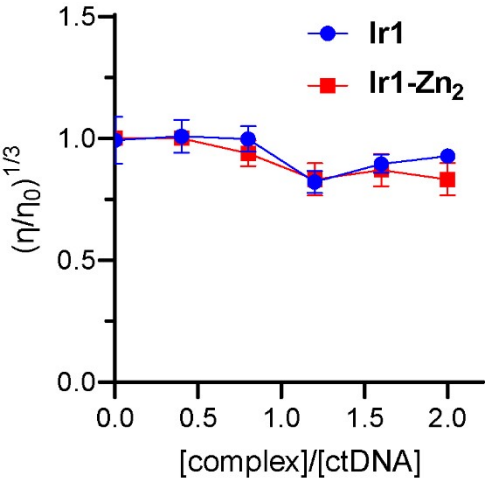

Figure S44. Effect of **Ir1** and **Ir1-Zn$_2$** on the relative viscosity of ct-DNA.

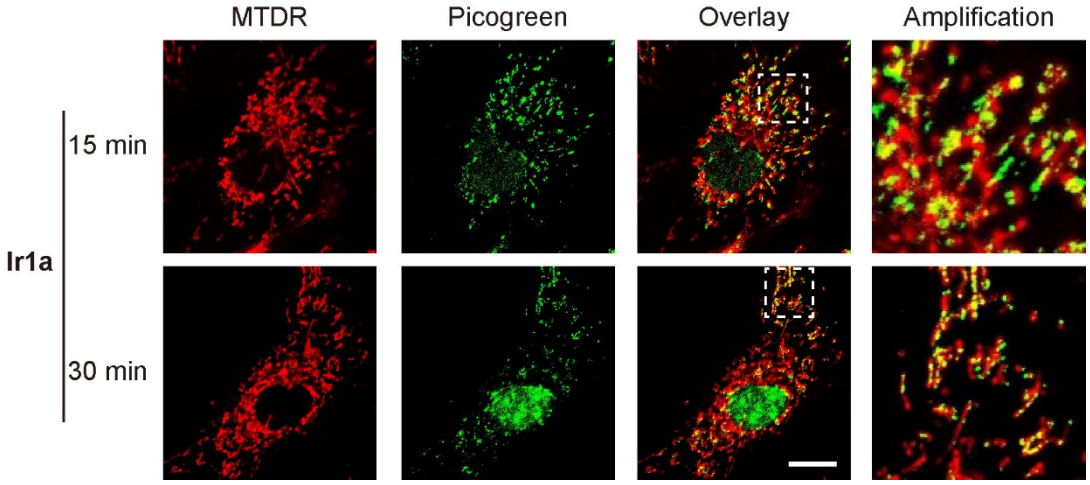

Figure S45. Colocalization of MTDR with PicoGreen in MDA-MB-231 cells. Cells were treated with **Ir1a** (2 µM) and incubated with PicoGreen (1 µg mL^{-1}, 15 min) and MTDR (100 nM, 15 min). **Ir1a**: λ_{ex}= 405 nm; λ_{em}= 600 ± 20 nm. PicoGreen: λ_{ex} = 488 nm, λ_{em} = 520 ± 20 nm. MTDR: λ_{ex} = 633 nm. λ_{em} = 660 ± 10 nm. Scale bar: 10 µm.

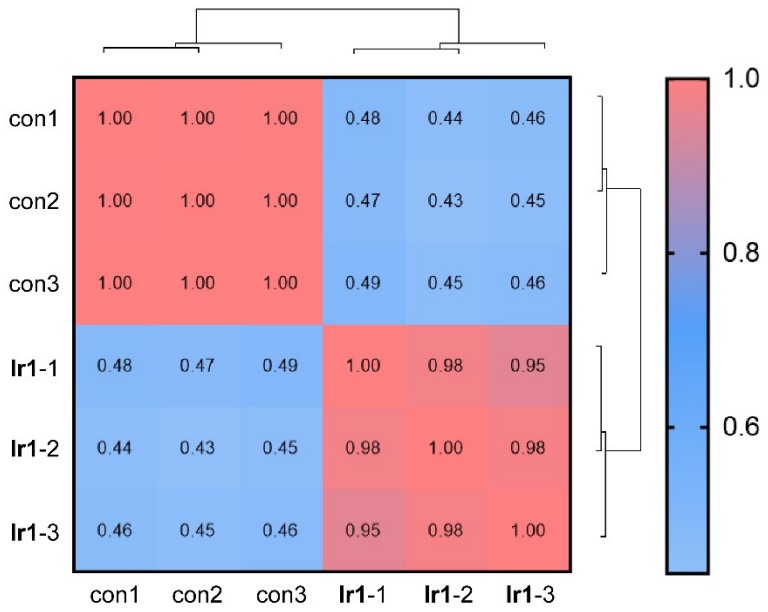

Figure S46. Heat map diagram of Pearson correlation coefficients between the RNA-seq samples.

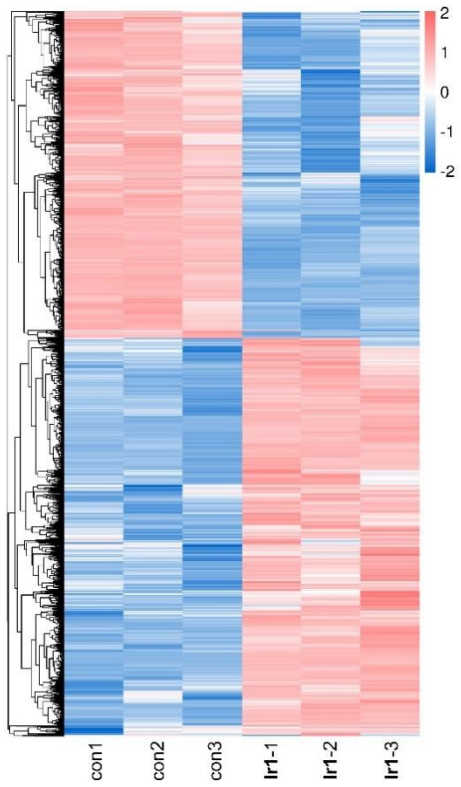

Figure S47. Cluster analysis and Heatmap displays the overview of the differentially expressed genes.

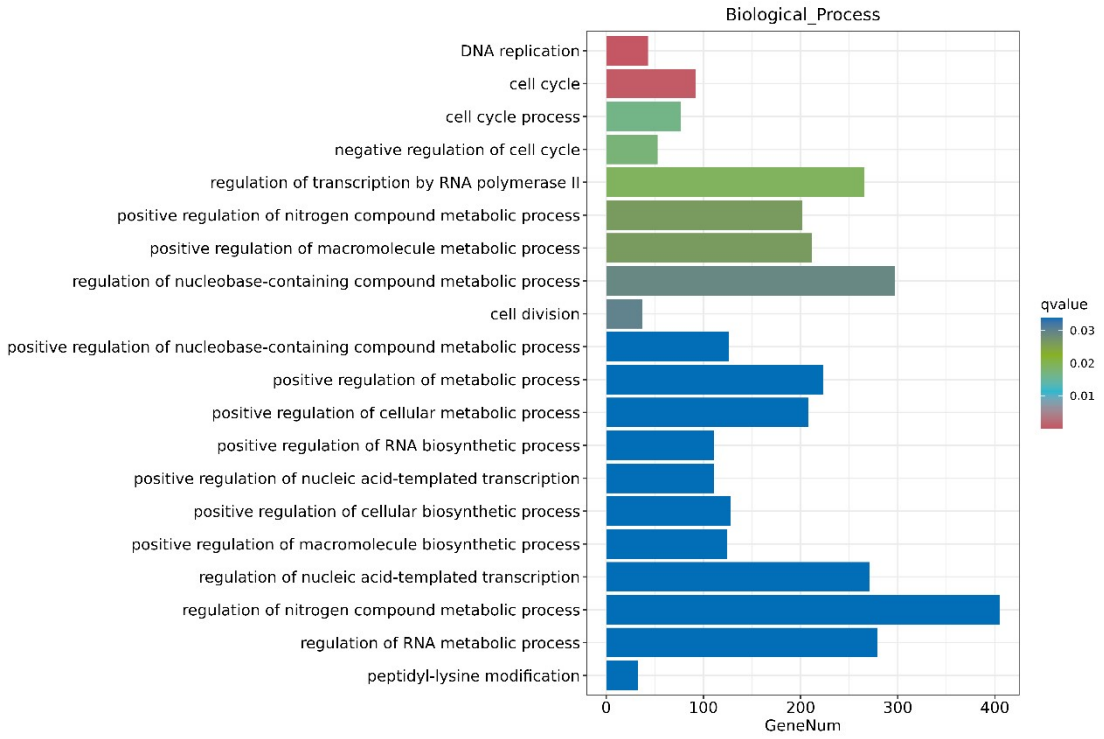

Figure S48. Gene Ontology categorization of biological process for assembled unigenes of the transcriptome induced by **Ir1**.

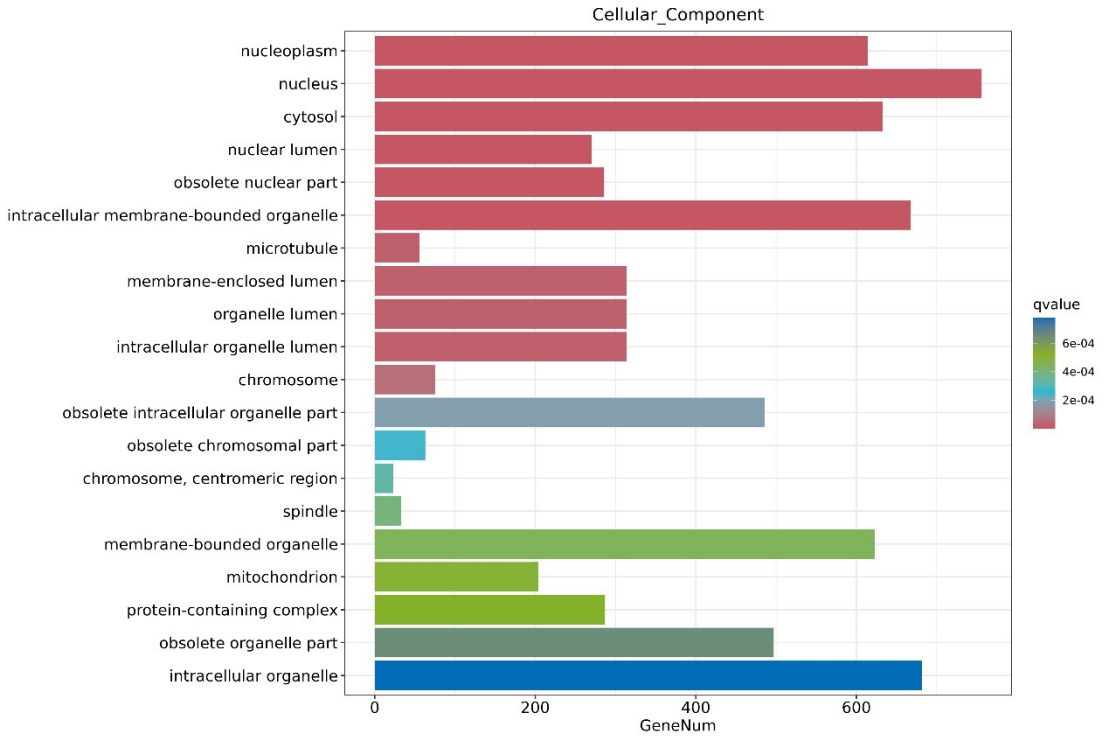

Figure S49. Gene Ontology categorization of cellular component for assembled unigenes of the transcriptome induced by **Ir1**.

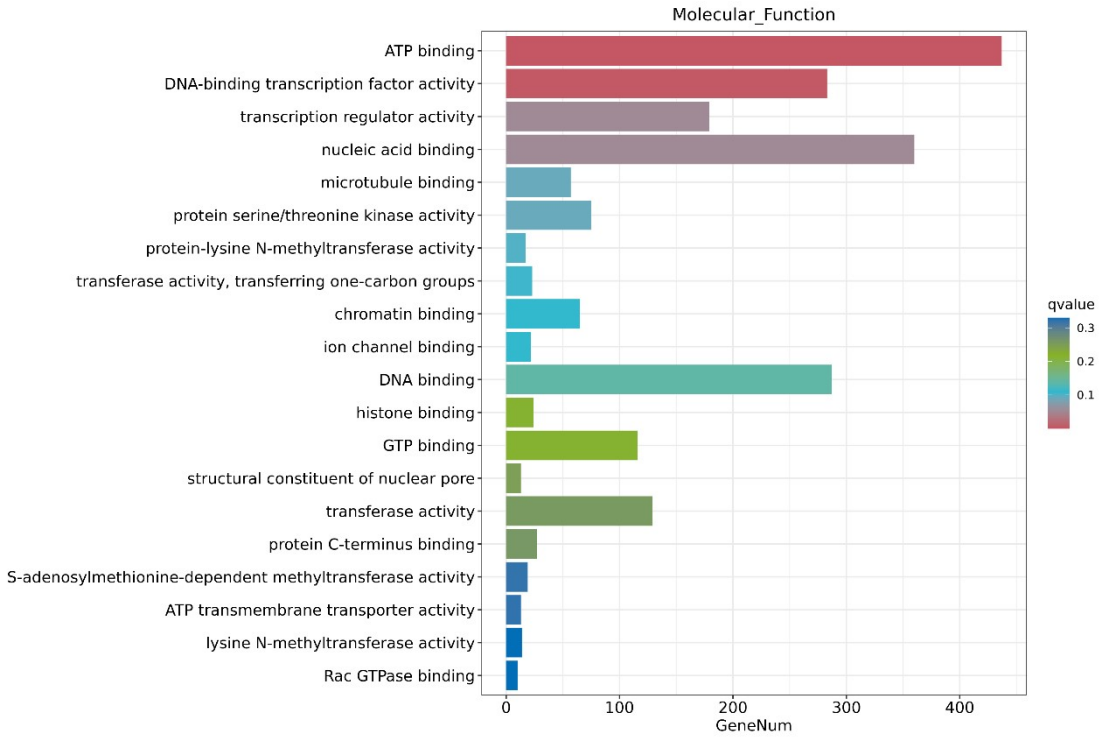

Figure S50. Gene Ontology categorization of molecular function for assembled unigenes of the transcriptome induced by **Ir1**.

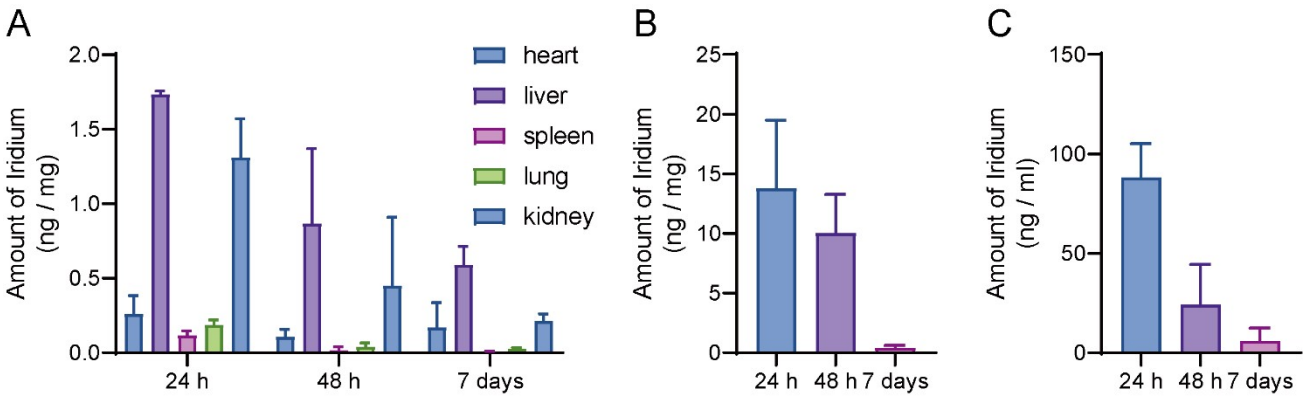

Figure S51. Iridium contents of main organs(A), tumors (B) and blood (C) measured by ICP-MS.

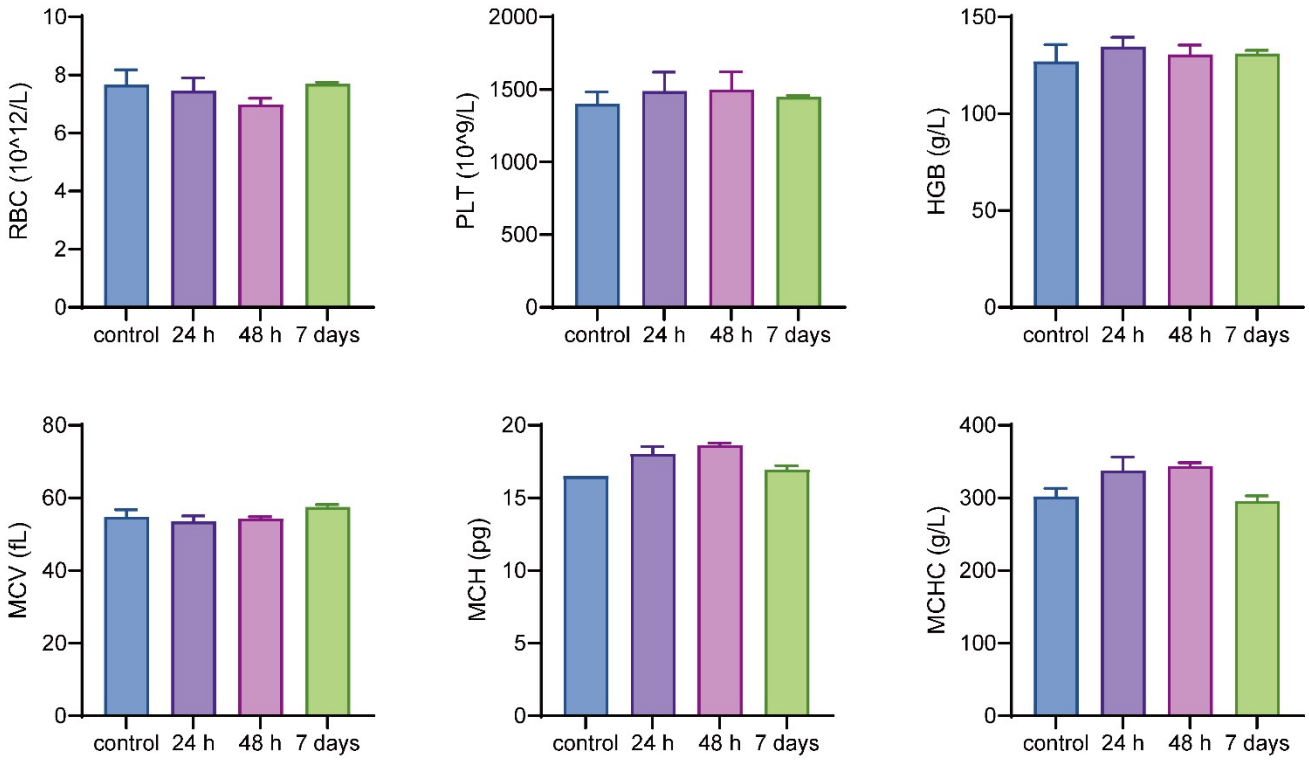

Figure S52. Routine blood test results from mice treated with **Ir1** (5 mg kg^{-1}), using tumor-bearing mice treated with PBS as controls. Abbreviation: RBC: red blood cell; PLT: platelets; HGB, hemoglobin; MCV, mean corpuscular volume; MCH, mean corpuscular hemoglobin; MCHC, mean corpuscular hemoglobin concentration. Data are shown as the mean ± SD, n = 3.

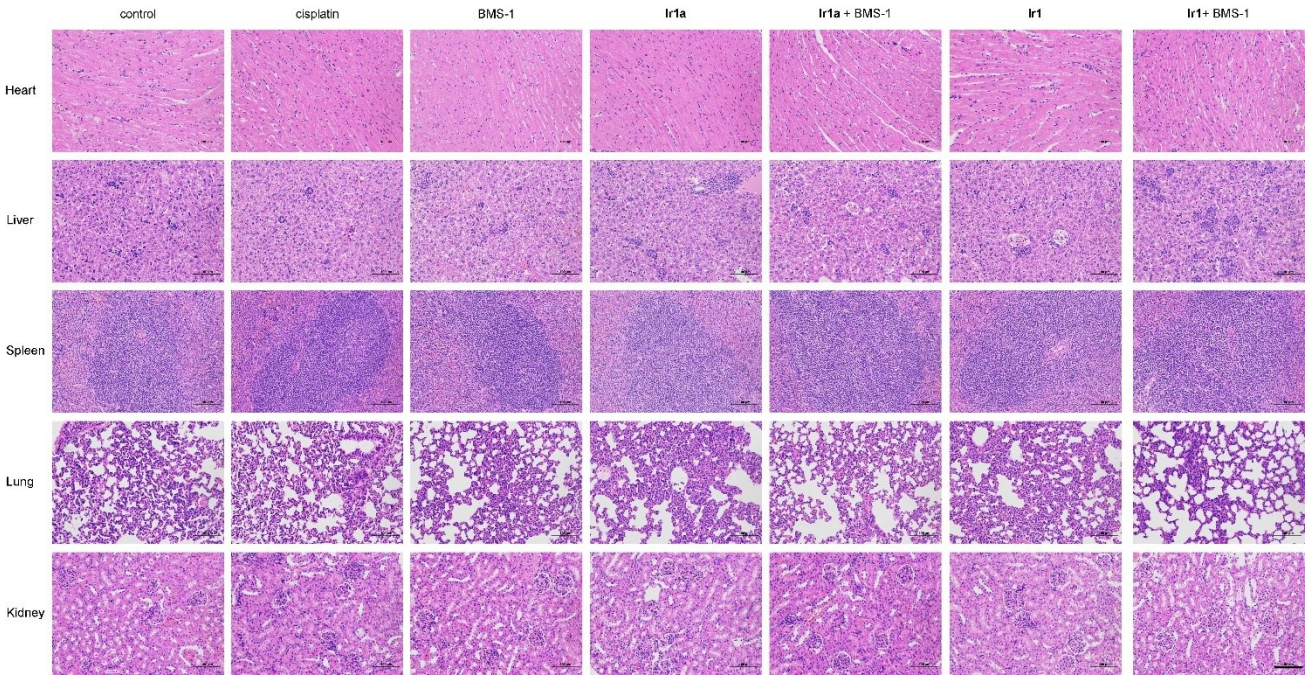

Figure S53. H&E staining of the main organs from mice with different treatment. Scale bars: 100 μm.

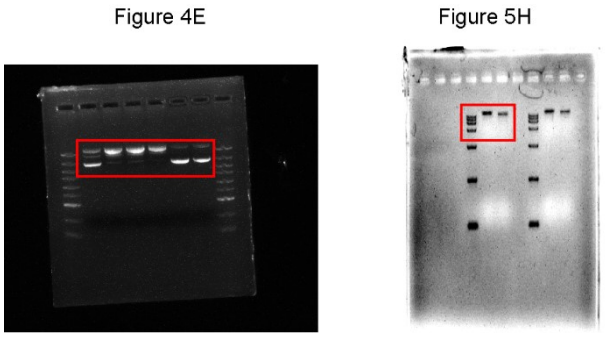

Figure S54. Raw images of agarose gel.

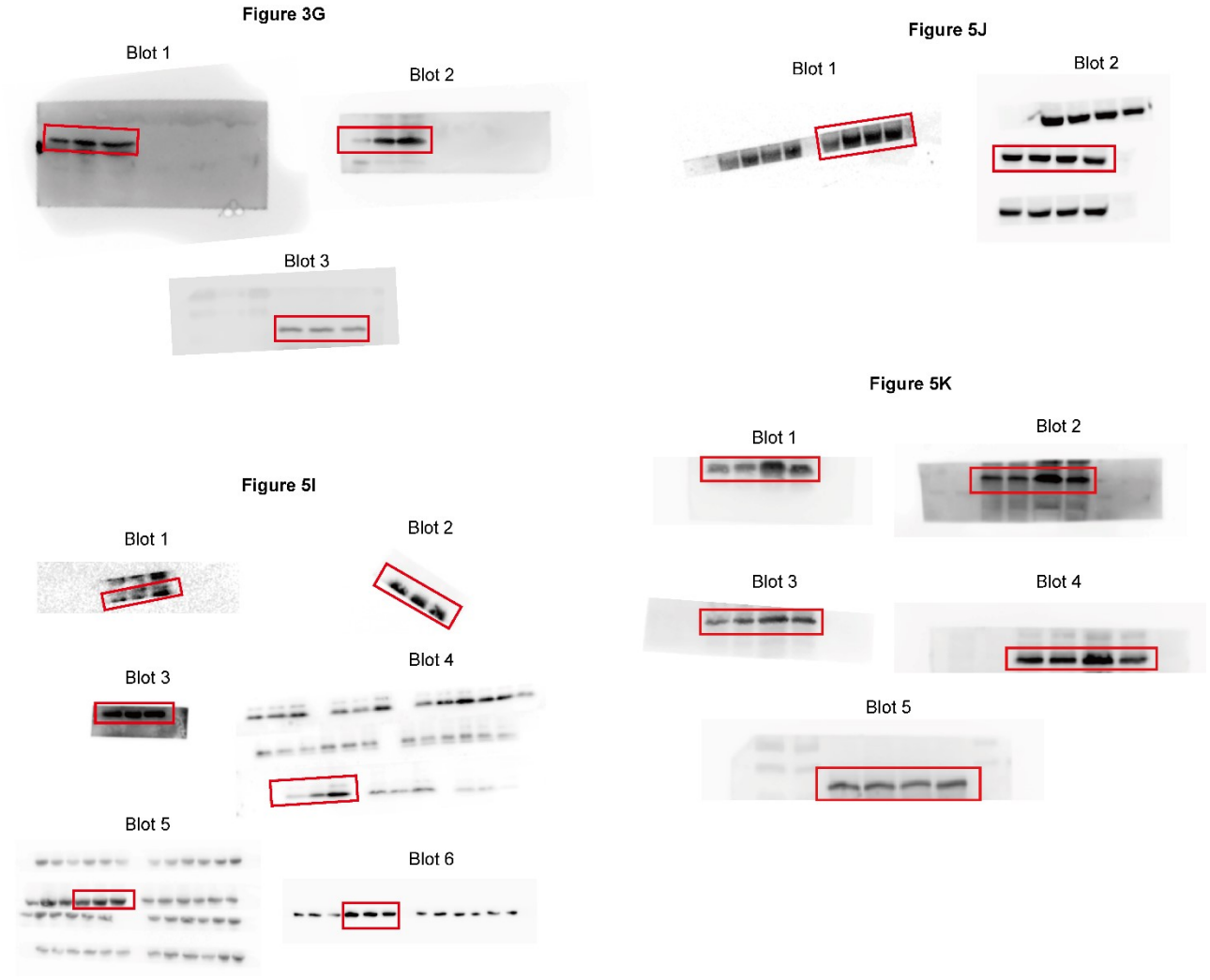

Figure S55. Raw images of western blot.

Table S1. The photophysical properties of **Ir1–Ir4** and **Ir1a–Ir4a** (20 μM) in degassed medium[a]

Compounds	Medium	$\lambda_{abs,\ max}$/nm	$\lambda_{em,\ max}$/nm	Φ_{em}[b]	τ/ns[c]
Ir1	CH_2Cl_2	410	613	0.036	/
	CH_3CN	407	604	0.11	/
	PBS	416	589	0.059	648.68 ± 5.26
Ir2	CH_2Cl_2	420	623	0.021	/
	CH_3CN	415	628	0.080	/
	PBS	425	602	0.15	700.50 ± 7.65
Ir3	CH_2Cl_2	361	546	0.041	/
	CH_3CN	359	538	0.036	/
	PBS	363	525	0.16	1485.53 ± 33.80
Ir4	CH_2Cl_2	416	631	0.022	/
	CH_3CN	412	629	0.032	/
	PBS	420	613	0.018	825.01 ± 20.14
Ir1a	CH_2Cl_2	410	598	0.14	/
	CH_3CN	409	602	0.071	/
	PBS	408	616	0.010	46.46 ± 1.83
Ir2a	CH_2Cl_2	418	627	0.052	/
	CH_3CN	415	638	0.043	/
	PBS	414	646	0.0031	100.82 ± 9.73
Ir3a	CH_2Cl_2	363	532	0.68	/
	CH_3CN	360	540	0.18	/
	PBS	360	552	0.14	797.10 ± 7.72
Ir4a	CH_2Cl_2	415	626	0.059	/
	CH_3CN	412	649	0.026	/
	PBS	408	649	0.0017	36.46 ± 1.57

[a]All emission decays were obtained on freshly prepared samples placed in quartz cuvettes. Samples were 2×10^{-5} M in concentration. [b]$[Ru(bpy)_3](PF_6)_2$ were used as the standard. PBS (Φ_{em} = 0.042),[9] CH_3CN (Φ_{em} = 0.062)[10] and CH_2Cl_2 (Φ_{em} = 0.059).[11] [c]All fittings are to a bi-exponential decay model.

Table S2. Lipophilicity of Ir(III) complexes

Compounds	Lipophilicity (log $P_{o/w}$)
Ir1	1.47
Ir2	3.15
Ir3	1.24
Ir4	2.26
Ir1a	-0.76
Ir2a	-0.03
Ir3a	-0.02
Ir4a	-0.27

Table S3. The numerical lifetime and fractional contribution values of **Ir1** in the presence of different molar ratios of Zn^{2+} in PBS buffer.

[Zn]/[Ir1]	τ_1	Rel_1/%	τ_2	Rel_2/%	τ
0	160.67 ± 1.69	28.74	845.52 ± 6.70	71.26	648.68 ± 5.26
0.2	177.29 ± 1.44	39.42	808.24 ± 7.95	60.58	559.52 ± 5.38
0.4	184.44 ± 1.51	52.27	733.03 ±10.95	47.73	446.26 ± 6.02
0.6	192.32 ± 2.31	61.25	648.69 ± 23.21	38.75	369.16 ± 10.41
0.8	198.04 ± 4.61	74.20	552.64 ± 68.96	25.80	289.54 ± 21.22
1.0	196.17 ± 2.61	76.79	482.38 ± 26.16	24.21	265.48 ± 8.31
1.2	162.78 ± 6.21	45.40	324.33 ± 13.52	54.60	250.99 ± 10.20
1.4	87.62 ± 4.68	10.21	259.49 ± 2.48	89.79	241.94 ± 2.71
1.6	145.05 ± 8.62	32.13	299.52 ± 11.46	67.87	249.89 ± 10.55
1.8	148.64 ± 9.04	33.41	300.72 ± 12.83	66.59	249.90 ± 11.56
2.0	70.74 ± 3.53	7.20	258.51 ±1.74	92.80	245.00 ± 1.87

Table S4. The numerical lifetime and fractional contribution values of **Ir2** in the presence of different molar ratios of Zn^{2+} in PBS buffer.

[Zn]/[Ir2]	τ_1	Rel_1/%	τ_2	Rel_2/%	τ
0	247.56 ± 11.90	17.32	795.39 ± 6.76	82.68	700.50 ± 7.65
0.2	179.68 ± 9.17	12.85	763.83 ± 5.15	87.15	688.77 ± 5.66
0.4	146.33 ± 6.84	12.93	757.16 ± 4.90	87.07	678.18 ± 5.15
0.6	105.92 ± 3.75	15.90	742.37 ± 4.85	84.10	641.18 ± 4.68
0.8	84.14 ± 2.10	24.39	716.53 ± 5.47	75.61	562.29 ± 4.65
1.0	75.24 ± 1.41	42.97	671.99 ± 7.80	57.03	415.57 ± 5.05
1.2	70.51 ± 1.16	61.93	615.60 ± 12.22	38.07	278.03 ± 5.37
1.4	72.44 ± 1.13	80.96	536.68 ± 22.90	19.04	160.83 ± 5.27
1.6	74.13 ± 0.85	92.11	612.35 ± 43.77	7.89	116.59 ± 4.24
1.8	71.88 ± 0.87	91.20	544.08 ± 37.10	8.80	113.43 ± 4.06
2.0	70.73 ± 0.96	89.44	513.72 ± 35.00	10.56	117.51 ± 4.56

Table S5. The numerical lifetime and fractional contribution values of **Ir3** in the presence of different molar ratios of Zn^{2+} in PBS buffer.

[Zn]/[Ir3]	τ_1	Rel_1/%	τ_2	Rel_2/%	τ
0	711.83 ± 15.12	59.01	2599.35 ±60.70	40.99	1485.53 ± 33.80
0.2	926.26 ± 17.25	72.47	2880.54 ±100.00	27.53	1464.28 ± 40.03
0.4	1024.08 ± 21.80	79.01	2663.45 ±144.23	20.99	1368.18 ± 47.50
0.6	1055.44 ± 29.35	77.81	2232.63 ±154.54	22.19	1316.66 ± 57.13
0.8	437.11 ± 79.18	7.8	1311.80 ± 16.05	92.20	1243.57 ± 20.97
1.0	602.93 ±112.09	5.31	1294.25 ±32.92	94.69	1251.88 ± 37.13
1.2	252.06 ± 86.92	1.46	1278.88 ± 6.22	98.54	1263.89 ± 7.40
1.4	197.11 ± 67.06	1.18	1282.32 ± 5.55	98.82	1269.52 ±6.28
1.6	287.05 ± 86.71	1.84	1288.53 ± 6.78	98.16	1270.11 ± 8.25
1.8	175.32 ± 74.82	0.91	1272.45 ±5.26	99.09	1262.47 ± 5.90
2.0	138.00 ± 53.29	0.88	1282.09 ± 5.04	99.12	1272.02 ± 5.47

Table S6. The numerical lifetime and fractional contribution values of **Ir4** in the presence of different molar ratios of Zn^{2+} in PBS buffer.

[Zn]/[Ir4]	τ_1	Rel_1/%	τ_2	Rel_2/%	τ
0	540.45 ± 8.89	72.60	1578.98 ± 49.96	27.40	825.01 ± 20.14
0.2	391.85 ± 10.76	51.82	1162.70 ± 28.56	48.18	763.24 ± 19.34
0.4	100.62 ± 3.76	23.51	824.59 ± 8.81	76.49	654.38 ± 7.63
0.6	78.26 ± 2.18	39.96	798.67 ± 12.37	60.04	510.80 ± 8.30
0.8	64.31 ± 1.13	77.64	681.52 ± 25.20	22.36	202.31 ± 6.51
1.0	60.81 ± 0.49	97.34	541.00 ± 106.91	2.66	73.58 ± 3.32
1.2	57.92 ± 0.93	94.77	187.59 ± 31.04	5.23	64.70 ± 2.50
1.4	62.35 ± 0.40	96.71	331.83 ± 44.27	3.29	71.22 ± 1.84
1.6	61.02 ± 0.53	94.58	204.91 ± 21.57	5.42	68.81 ± 1.67
1.8	62.16 ± 0.38	96.14	387.16 ± 46.41	3.86	74.70 ± 2.16
2.0	60.25 ± 0.61	93.48	184.22 ± 17.67	6.52	68.33 ± 1.72

Table S7. The TD-DFT calculated energy levels of **Ir1**.

	Energy (eV)	**Transition configuration**
S_1	2.4042	H → L 98.9%
S_2	3.1221	H → L+1 97.2%
S_3	3.1850	H-4 → L 58.6% H-2 → L 31.8%
S_4	3.2183	H-1 → L 44.4% H → L+2 34.3% H-5 → L 18.0%
S_5	3.2894	H → L+2 62.0% H-1 → L 30.0%
T_1	2.3521	H → L 96.2%
T_2	2.4922	H-8 → L 27.2% H-2 → L 20.7% H-4 → L 14.6% H-6 → L 8.6%
T_3	2.7099	H → L+1 65.9% H-1 → L+2 12.0%
T_4	2.7842	H → L+2 50.6% H-1 → L+1 20.5%
T_5	2.9307	H-1 → L 48.8% H-5 → L 40.1%

Table S8. Cytotoxicity (IC_{50}, μM) of the tested compounds on MDA-MB-231 cell lines[a]

Complex	**Ir1a**	**Ir2a**	**Ir3a**	**Ir4a**
MDA-MB-231	6.3 ± 0.7	6.0 ± 0.4	4.7 ± 0.6	3.3 ± 0.2
HeLa	1.54 ± 0.42	1.08 ± 0.10	1.21 ± 0.14	1.42 ± 0.65

[a] Cells were incubated with the compounds for 72 h. Data are presented as the means ± standard deviations (SD).

Table S9. Docked free energy range of **Ir1** with ds-DNA (PDB: 5t4w)

Number of AutoDock clusters[a]	Docked free energy range of docked structures (kcal mol^{-1})	Cluster rank[b]	Docked free energy (kcal mol^{-1})
50	-7.85 to -9.14	1	-9.14
		2	-9.14
		3	-8.52
		4	-8.47
		5	-8.12
		6	-8.11
		7	-7.95
		8	-7.94
		9	-7.94
		10	-7.85

[a] Number of GA runs are shown in parentheses. [b] The cluster rank is the absolute ranking as determined by the docked free energy defined by AutoDock.

Table S10. Docked free energy range of **Ir1-Zn** with ds-DNA (PDB: 5t4w)

Number of AutoDock clusters[a]	Docked free energy range of docked structures (kcal mol^{-1})	Cluster rank[b]	Docked free energy (kcal mol^{-1})
50	-9.11 to -11.04	1	-11.04
		2	-10.74
		3	-10.30
		4	-9.58
		5	-9.51
		6	-9.49
		7	-9.48
		8	-9.25
		9	-9.16
		10	-9.11

[a] Number of GA runs are shown in parentheses. [b] The cluster rank is the absolute ranking as determined by the docked free energy defined by AutoDock.

Table S11. Zn^{2+} regulatory protein related genes dysregulated in **Ir1**-treated MDA-MB-231 cells.

#ID	Symbol	log_2(Fold Change)	regulated
ENSG00000138821	SLC39A8	-1.49334	down
ENSG00000112473	SLC39A7	0.84669	up
ENSG00000115194	SLC30A3	1.855609	up
ENSG00000104154	SLC30A4	-1.03296	down
ENSG00000170385	SLC30A1	5.032361	up
ENSG00000014824	SLC30A9	-0.62122	down
ENSG00000141873	SLC39A3	-0.84895	down
ENSG00000198417	MT1F	5.805033	up
ENSG00000109610	SOD3	0.783984	up
ENSG00000187193	MT1X	2.952612	up
ENSG00000169715	MT1E	2.516787	up
ENSG00000205362	MT1A	1.408797	up
ENSG00000242114	MTFP1	-0.65609	down
ENSG00000188786	MTF1	0.795277	up
ENSG00000146410	MTFR2	-1.07031	down
ENSG00000125148	MT2A	1.446677	up

Table S12. OXPHOS-related genes dysregulated in **Ir1**-treated MDA-MB-231 cells.

#ID	Symbol	log_2(Fold Change)	regulated
ENSG00000198888	MT-ND1	-2.73786	down
ENSG00000198763	MT-ND2	-2.81509	down
ENSG00000198840	MT-ND3	-3.00117	down
ENSG00000198886	MT-ND4	-2.99284	down
ENSG00000212907	MT-ND4L	-3.6268	down
ENSG00000198786	MT-ND5	-4.26752	down
ENSG00000198695	MT-ND6	-4.32626	down
ENSG00000198804	MT-CO1	-4.58623	down
ENSG00000198712	MT-CO2	-2.11304	down
ENSG00000198938	MT-CO3	-2.14785	down
ENSG00000198727	MT-CYB	-2.26265	down
ENSG00000198899	MT-ATP6	-2.27031	down
ENSG00000228253	MT-ATP8	-2.88307	down

Table S13. The primer sequences studied in qPCR.

Appellative	**Sequence**	**Appellative**	**Sequence**
SLC39A1 F	TGAGCCTAGTAAGCTGTTTCGC	SLC30A6 F	AGGAAACCTAGCCCTGTCTATT
SLC39A1R	CAGGGCCTCATCTATGGCA	SLC30A6 R	CAAAAAGCGTTCTGCACTTTCT
SLC39A2 F	TGGGCAGTGTTCTCCATACTA	SLC30A7 F	TCTCGGGCTGGTTTAGGTCTA
SLC39A2 R	AATAAAGGCCATGAAGGCAAAAC	SLC30A7 R	ACAAAAGCGAAAGAGAGGTTCA
SLC39A3 F	TGCTCCCCGTGAAGATCATC	SLC30A8 F	TGAGTACGCCTATGCCAAGTG
SLC39A3 R	TCCAAAGGTGTTGCAGAGAGA	SLC30A8 R	CTGGTCAGGTCAATTAAGAGGTG
SLC39A4 F	TGGTCTCTACGTGGCACTC	SLC30A9 F	AGGGAGTATGGCTCAAAGTACA
SLC39A4 R	GGGTCCCGTACTTTCAACATC	SLC30A9 R	GGGACTTCGTCGTCTGATTTTTC
SLC39A5 F	GGTCCCCAGTGAGTCATCTG	SLC30A10 F	ACCGTGTTCGCAAACGTAG
SLC39A5 R	GCCAGGTAATGGTTCTGCTCC	SLC30A10 R	TCACATGCAAAAGTACACCTCTG
SLC39A6 F	ATGCAAGTCACCACCATAGTCA	MT1A F	ATGGACCCCAACTGCTCCT

SLC39A6 R	ACGTGGAATCAAAATAGGCACT	MT1A R	GCACTTCTCTGATGCCCCTT
SLC39A7 F	GGACACGCTCACAGTCATACA	MT1B F	ATGGATCCCAACTGCTCCTG
SLC39A7 R	CTCCTCGCCTCTTCTGAACC	MT1B R	CAGCGGCACTTCTCTGATGA
SLC39A8 F	ATGCTACCCAAATAACCAGCTC	MT1E F	TCAGGTTGGGAGGGAACTCAA
SLC39A8 R	ACAGGAATCCATATCCCCAAACT	MT1E R	GAAAGCCTGGAGAGGGAATGA
SLC39A9 F	CATGCTGGCTTAGAGCGGAAT	MT1F F	TGGTTCCTGCAAGTGCAAAGAGTG
SLC39A9 R	TGGTGCTGCCAATGCAAAGA	MT1F R	TAGCCACAGCCCCAGACCATG
SLC39A10 F	CACCATCGTTTGCATCATCATC	MT1G R	GCACCTCCTGCAAGAAGAGCTG
SLC39A10 R	GCTCACTGGGAGTAATGGAATC	MT1G R	CACTTCTCCGATGCCCCTTTGC
SLC39A11 F	CAGCTCTCGTGTTCGTATTCTC	MT1M F	GCACCTCCTGCAAGAAGAGCTG
SLC39A11 R	TCAGCCAAGTAGACAAAAGCC	MT1M R	TGCAGTTCTCCAACGTCCCTTTG
SLC39A12 F	TTCTTCTACTCAGCCGTGTTTTT	MT1H F	GCACCTCCTGCAAGAAGAGCTG
SLC39A12 R	GTCACCAGCAGAGAGAACCT	MT1H R	GCACTTCTCTGACGCCCCTTTG
SLC39A13 F	TCAGCGGCTACCTCAACCT	MT1X F	GGACCCCAACTGCTCCTGCTC
SLC39A13 R	AGGAGCCCGATCTTCTTGCT	MT1X R	CACACTTGGCACAGCCCACAG
SLC39A14 F	GAGGCTCACGCTTCATCCC	MT2A F	TGCAAGAAAAGCTGCTGCTCCTG
SLC39A14 R	CCCTCGCCATACCGATGTATTA	MT2A R	CACTTGTCCGACGCCCCTTTG
SLC30A1 F	GGACAACTTAACATGCGTGGA	MT3 F	GCAAGTGCGAGGGATGCAAATG
SLC30A1 R	ACACAAAAATCCCCTTCAGAACA	MT3 R	GTCCTTGGCACACTTCTCACACTC
SLC30A2 F	CGGCAATCCGGTCATACAC	MTF-1 F	CCTCAGCACAATTTCACCAGCAATC
SLC30A2 R	AGATGGCAGAGGCTACATACAG	MTF-1 R	GCGGAACATCACTGACTGACTCTG
SLC30A3 F	CAACCTGTTAATGGCCTTTGTG	SOD1 F	GGTGGGCCAAAGGATGAAGAG
SLC30A3 R	CTCCAGCGGTGCATACTCT	SOD1 R	CCACAAGCCAAACGACTTCC
SLC30A4 F	TGGAAGCGCCTCAAATCTATG	SOD2 F	TTTCAATAAGGAACGGGGACAC
SLC30A4 R	CAGTAAGGAATCATCGTCGGC	SOD2 R	GTGCTCCCACACATCAATCC
SLC30A5 F	TCTATGGCGTGCTGACCAATA	SOD3 F	ATGCTGGCGCTACTGTGTTC
SLC30A5 R	GCATGGCTATGGCATGGTG	SOD3 R	CTCCGCCGAGTCAGAGTTG
CYTb F	ACCCCCTAGGAATCACCTCC	CYTb R	GCCTAGGAGGTCTGGTGAGA
ND6 F	GGAGGATCCTATTGGTGCGG	ND6 R	CCTATTCCCCCGAGCAATCTC

ND5 F	TGGCAGCCTAGCATTAGCAG	ND5 R	GATAGGGCTCAGGCGTTTGT
ND4 F	ACACAATGGGGCTCACTCAC	ND4 R	CCGGTAATGATGTCGGGGTT
ND4L F	TACTAGTTTTTGCCGCCTGC	ND4L R	AGCATTGGAGTAGGCTTAGGTT
ND3 F	GCCCTCCTTTTACCCTTACCA	ND3 R	GGCCAGACTTAGGGCTAGGA
COX3 F	ACCCTCCTACAAGCCTCAGA	COX3 R	TGACGTGAAGTCCGTGGAAG
ATPase6 F	GAAGCGCCACCCTAGCAATA	ATPase6 R	GCTTGGATTAAGGCGACAGC
ATPase8 F	CACAAACTACCACCTACCTCCC	ATPase8 R	GGGCAATGAATGAAGCGAAC
COX2 F	GCTGTCCCCACATTAGGCTT	COX2 R	ACCGTAGTATACCCCCGGTC
COX1 F	CCCCGATGCATACACCACAT	COX1 R	TCGAAGCGAAGGCTTCTCAA
ND2 F	AGCACCACGACCCTACTACT	ND2 R	CATTTGGGCAAAAAGCCGGT
ND1 F	TAACGCACTCTCCCCTGAAC	ND1 R	GTAGCGGAATCGGGGGTATG
mtDNA F	CAC CCA AGA ACA GGG TTT GT	mtDNA R	TGG CCA TGG GTA TGT TGT TA
nDNA F	TGC TGT CTC CAT GTT TGA TGT ATC T	nDNA R	TCT CTG CTC CCC ACC TCT AAG

Reference

1. S. Sprouse, K. A. King, P. J. Spellane and R. J. Watts, *J. Am. Chem. Soc.*, 1984, **106**, 6647.
2. A. Ojida, M.-a. Inoue, Y. Mito-oka, H. Tsutsumi, K. Sada and I. Hamachi, *J. Am. Chem. Soc.*, 2006, **128**, 2052.
3. H.-B. Kim, Y. Li and M. H. Hyun, *Bull. Korean Chem. Soc.*, 2013, **34**, 653.
4. H.-b. Kim, Y. Liu, D. Nam, Y. Li, S. Park, J. Yoon and M. H. Hyun, *Dyes Pigm.*, 2014, **106**, 20.
5. R.-R. Ye, C.-P. Tan, L. He, M.-H. Chen, L.-N. Ji and Z.-W. Mao, *Chem. Commun.*, 2014, **50**, 10945.
6. M. G. Colombo and H. U. Guedel, *Inorg. Chem.*, 1993, **32**, 3081.
7. F. Lafolet, S. Welter, Z. Popović and L. D. Cola, *J. Mater. Chem.*, 2005, **15**, 2820.
8. M. Bandini, M. Bianchi, G. Valenti, F. Piccinelli, F. Paolucci, M. Monari, A. Umani-Ronchi and M. Marcaccio, *Inorg. Chem.*, 2010, **49**, 1439.
9. J. Van Houten and R. J. Watts, *J. Am. Chem. Soc.*, 1976, **98**, 4853.
10. D. S. Tyson and F. N. Castellano, *J. Phys. Chem.*, 1999, **103**, 10955.
11. D. Pucci, A. Bellusci, A. Crispini, M. Ghedini, N. Godbert, E. I. Szerb and A. M. Talarico, *J. Mater. Chem.*, 2009, **19**, 7643.
12. X.-L. Li, M.-F. Wang, L.-Z. Zeng, G.-K. Li, R.-Y. Zhao, F.-D. Liu, Y. Li, Y.-F. Yan, Q. Liu, Z. Li, H. Zhang, X. Ren and F. Gao, *Angew. Chem., Int. Ed.*, 2024, **63**, e202402028.
13. H. A. Benesi and J. H. Hildebrand, *J. Am. Chem. Soc.*, 1949, **71**, 2703.
14. R. B. Nair, E. S. Teng, S. L. Kirkland and C. J. Murphy, *Inorg. Chem.*, 1998, **37**, 139.
15. X.-Z. Feng, Z. Lin, L.-J. Yang, C. Wang and C.-L. Bai, *Talanta*, 1998, **47**, 1223.
16. W. L. DeLano, PyMOL(TM) Molecular Graphics System, Version 1.7.*Journal*, 2009.
17. C. I. Bayly, P. Cieplak, W. Cornell and P. A. Kollman, *J. Phys. Chem.*, 1993, **97**, 10269.
18. G. M. Morris, R. Huey, W. Lindstrom, M. F. Sanner, R. K. Belew, D. S. Goodsell and A. J. Olson, *J. Comput. Chem.*, 2009, **30**, 2785.
19. G. M. Morris, D. S. Goodsell, R. S. Halliday, R. Huey, W. E. Hart, R. K. Belew and A. J. Olson, *J. Comput. Chem.*, 1998, **19**, 1639.
20. R. Laskowski, LigPlot^{+} Version 1.4.5.*Journal*, 2009.
21. Y.-Y. Ling, X.-Y. Xia, L. Hao, W.-J. Wang, H. Zhang, L.-Y. Liu, W. Liu, Z.-Y. Li, C.-P. Tan and Z.-W. Mao, *Angew. Chem. Int. Ed.*, 2022, **61**, e202210988.
22. Y.-Y. Ling, Z.-Y. Li, X. Mu, Y.-J. Kong, L. Hao, W.-J. Wang, Q.-H. Shen, Y.-B. Zhang and C.-P. Tan, *Eur. J. Med. Chem.*, 2024, **275**, 116638.
23. X. X. Su, B. Liu, W. J. Wang, K. Peng, B. B. Liang, Y. Zheng, Q. Cao and Z. W. Mao, *Angew. Chem. Int. Ed.*, 2023, **62**, e202216917.
24. Y. Zheng, X.-X. Chen, D.-Y. Zhang, W.-J. Wang, K. Peng, Z.-Y. Li, Z.-W. Mao and C.-P. Tan, *Chem. Sci.*, 2023, **14**, 6890.